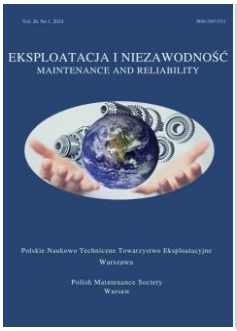

Eksploatacja i Niezawodnosc – Maintenance and Reliability

Volume 26 (2024), Issue 1

journal homepage: http://www.ein.org.pl

Article citation info:
Łagoda T, Małecka J, Małys S, Derda S, Kuś J, Krysiński P, Fatigue fracture cross-sections after cyclic tests with a combination of cyclic bending and torsion of samples made of aluminum alloy 6060, Eksploatacja i Niezawodnosc – Maintenance and Reliability 2024: 26(1) http://doi.org/10.17531/ein/176203

Fatigue fracture cross-sections after cyclic tests with a combination of cyclic bending and torsion of samples made of aluminum alloy 6060

Indexed by:

Tadeusz Łagoda[a,*], Joanna Małecka[a], Slawomir Małys[a,b], Szymon Derda[a], Juliusz Kuś[a], Paweł Krysiński[b]

[a] Opole University of Technology, Poland
[b] RFWW "RAWAG" Sp. z o. o., Poland

Highlights

- Static and fatigue strength of aluminum alloy 6060 after T6 and T64 treatment.
- Safe windows and doors in railway cars.
- Topography of 6060 aluminum alloys after various treatments.
- Fatigue fracture topography of 6060 aluminum alloys under various loads.

Abstract

The paper presents the results of fatigue tests of the 6060 aluminum alloy. The test material was taken from the profiles used for the production of side windows and external doors of the passenger trains by the RAWAG company. The tests were carried out for cyclic loads with pure bending, pure torsion, and two combinations of bending and torsion. Fatigue tests were performed at zero mean values. Using scanning electron microscopy, a fractographic analysis was made, which is a supplementary basic for considerations about the mechanism of initiation and development of fatigue cracks. Based on the appearance of individual zones and the characteristics of cracks, a picture of the behavior of the material under specific conditions was obtained. Finally, the plastic property of fatigue cracks was indicated.

Keywords
aluminium 6060, bending and torsion, fatigue, fracture plane, fractography

1. Introduction

Environmental protection standards and safety considerations force the transport industry to search for the most optimal materials. Since the 1970s, the use of aluminum and its alloys has been intensified. Commonly used steel components in transport directly impact the high weight of these vehicles. Any injuries to people involved in a collision with such a powerful machine may have fatal consequences. To minimize them, a better solution is aluminum alloys, which can absorb energy, thanks to which the components will bend smoothly in the event of a collision, thus protecting passengers.

Using aluminum alloys is becoming relatively common because it is a relatively cheap and light material. Due to their characteristics, aluminum alloys are slowly replacing popular construction materials. This results in energy savings during operation.

Operating conditions include frequently occurring variable loads on the material. It should be noted, however, that in this context, aluminum alloys are less known than steel. Therefore, it is necessary to analyze aluminum alloys in terms of fatigue using various heat treatments to obtain reliable elements and,

(*) Corresponding author.
E-mail addresses: T. Łagoda (ORCID: 0000-0002-2815-3311) t.lagoda@po.opole.pl, J. Małecka (ORCID: 0000-0003-0974-9328) j.malecka@po.edu.pl, S. Małys (ORCID: 0000-0003-3365-2809) slawomir.malys@student.po.edu.pl, S. Derda (ORCID: 0000-0002-6340-6425) szymon.derda@student.po.edu.pl, J. Kuś (ORCID: 0000-0002-9273-8656) j.kus@po.edu.pl, P. Krysiński (ORCID: 0009-0000-1791-1183) pawel.krysinski@schaltbau-rawag.com

consequently, entire devices during the assumed operation. When using aluminum alloys for structural elements, attention should be paid to the long-term reliability of the components, i.e., such structures must withstand a very large number of cycles (VHCF). It was found [22] that, unlike steel, aluminum alloys in this range show a linear relationship between the stress amplitude and fatigue life. This work presents fatigue tests for 2024-T351, 6061, and AlZnMgCu1.5-T66 aluminum alloys.

Review works increasingly attempt to systematize knowledge regarding using aluminum alloys in means of transport, including railway transport. In [15], a critical review was made of the impact of fatigue on structures made of aluminum alloys and the effect of this fatigue on both design and service. In another work [37], attention was paid to the use of aluminum alloys in transport systems, taking into account modern technologies. These and other works (e.g. [14, 33]) demonstrated the development of high-speed trains, among others, through lightweight structures mainly based on aluminum alloys. It was also found [14, 36] that the microstructure of the used aluminum alloys has a significant impact on their properties and, as a result, on the use of aluminum alloys, taking into account, in particular, the fatigue strength.

An important aspect is determining the operational durability of aircraft structures, where a significant part of the elements are made of aluminum alloys. In [28], the fatigue strength of the 7050-T7451 aluminum alloy was analyzed. The work positively verified the model for assessing fatigue life in the HCF range under variable amplitude loads.

Of all means of transport, the use of aluminum alloys in rail transport is growing the fastest. When designing various structures, care should be taken to ensure their lightness has been known for some time. The manual [10] indicates that aluminum or composite elements should be used instead of steel elements instead of traditional wagon body structures. Often, they must also be layered structures consisting of various materials.

This is very important in rail transport. In the case of Maglev trains in China, speeds reach 600 km/h [16]. Lightweight bodies are made of 6082 T6 aluminum alloy. Accurate fatigue life calculations after the Shanghai accident showed that the predicted fatigue life decreased from 34.1 to 19.7 years. This analysis was performed based on fracture mechanics, where an initial crack of 3 mm was assumed.

The importance of testing the entire aluminum car body, both static and fatigue, was highlighted in, among others, the paper [35]. Fatigue tests were performed with four-point bending. Whole aluminum elements and individual welded joints were analyzed. The analyzed aluminum alloy is 6005-T6. Based on the research, it was found that the initiation of fatigue cracks occurs in the welded joints in the middle part of the wagons.

During the operation of railway vehicles, numerous micro-cracks occur due to fatigue, which weakens the fatigue life. In [43], it was shown that it is possible to carry out repair welding during planned inspections to ensure the appropriate reliability of trains in operation. Based on experimental tests, it has been shown that the welded joints made of the A7N01 aluminum alloy increase static and fatigue properties.

The vibration of high-speed train bogies frames is a natural phenomenon. This may result in fatigue cracking and should be prevented during operation. The paper [42] analyzed the behavior of high-speed trains in China, which move at a speed of 350 km/h. The work demonstrated the compliance of the FE model with bogie frame experimental tests. The analysis demonstrated allowed the design of safe and reliable high-speed trains at high speeds during their operation. Similar full-scale analyses were presented in [29]. Fatigue tests were performed using service loads with various load levels. The proposed ALT research method turned out to be correct when designing a welded bogie frame structure for high-speed trains.

The safety of various components of high-speed trains is critical. Due to the simultaneous increase in speed, structures are becoming lighter due to, among other things, the introduction of aluminum elements into the structure. The fatigue properties of aluminum alloys are less known than traditional steels. The work [39] presents the use of cast aluminum alloy in a gearbox. Strength analysis, performed using computational and experimental models, and surface analysis showed that the casting technology reduced porosity, enabling it to be used in the operation of high-speed trains.

In the work [17], attention was paid to the influence of microstructure, porosity, and fatigue strength on A7N01S-T5 aluminum alloy welded joints in high-speed trains [17]. Proper

execution of joints ensures better properties of welded structures, which translates into increased durability and reliability during the operation of light high-speed trains built based on aluminum alloys.

As you can see, lightweight structures are now very important because they reduce energy consumption during operation. The heaviest weight is the car body. In [31], an attempt was made to optimize such a structure. Thin-walled structures made of aluminum alloys subjected to operational loads were analyzed.

It must be remembered that comparing the static strength of various materials cannot be translated into fatigue properties. Therefore, there needs to be more appropriate approaches. This also applies to different heat treatments of aluminum alloys.

The FEM analysis of a load-bearing beam in a high-speed train made of cast aluminum [40] showed that the maximum stress loads were located in the seat support band. Experimental cyclic fatigue tests with a durability of 10^7 cycles did not reveal any cracks on the surface.

In mechanical structures, weight reduction is sought to save both the material used, which affects the costs, and energy consumption to drive the design. This effect can be obtained by using lightweight materials or their appropriate shape. It is also possible to use both methods simultaneously. Regarding lightweight materials, aluminum alloys have been used for a long time, and composites have been used more often in recent years. Rail transport consumes significant energy needed for propulsion. And this causes substantial transport costs. This is related to both energy consumption and infrastructure load. Therefore, where possible, lightweight materials are used and shaped accordingly. Windows and doors installed in passenger trains, the glass supporting structures are made of aluminum alloy profiles. When selecting the material, an alloy's metal forming method is considered: cast, sheet, or extruded profile. Window and door structures are currently made of extruded profiles. Exemplary door and window structures of aluminum alloy 6060 are shown in Figs. 1 and 2.

Fig.1. Door structure made of 6060 aluminum alloy.

Fig.2. Window structure made of 6060 aluminum alloy.

When designing aluminum structures and selecting the material, the following factors should be taken into account: purpose, i.e., in what conditions the element will work [41], further processing [19-20, 32, 38], strength, stiffness and elasticity [8, 21, 32], corrosion resistance [34], type of decorative coating or weldability [26].

For extruded profiles, alloys from the 6XXX group are mainly used [2]. During the alloy selection, the heat treatment process is also determined, which affects the requirements for

the material from which a given element or structure is made. The most commonly used treatment methods are:

- T4 - product oversaturated and naturally aged as needed,
- T5 - product cooled down from increased temperature and artificially aged,
- T6 - oversaturated and artificially aged,
- T64 - supersaturated and artificially aged at ground temperature,
- T7 - supersaturated and artificially aged (stabilized).

Treatment methods such as T4, T6, and T64 are often used for structures.

As mentioned earlier, aluminum alloys from the 6XXX group are used for structures made of profiles, with particular emphasis on the 6060 aluminum alloy. The main compositions of aluminium 6XXX are Zn and Mg. However, in the literature, only some studies analyze this material's strength and structure, taking into account various factors affecting the subsequent operation of this material. Few papers also show the fractography of the material structure after destruction, with particular emphasis on the effect of material fatigue.

In [21], the properties of the 6060 aluminum alloy were determined. This material was found to have high tensile strength, yield strength, and hardness. However, it is characterized by relatively low ductility.

The paper [38] shows that the influence of heat treatment on the strength of aluminum alloy was analyzed.

It has been shown that the T6 state increases the fatigue strength by about 30% compared to the T4 state.

In [32], a model for estimating the fatigue life of extruded elements made of aluminum alloy 6060 was developed. The analysis was based on tests of various geometries of the tested bars (rectangular cross-section with smooth surfaces and cavities and whole rectangular cross-section). Multiple treatments were also used: T1 and T4. As a result, it was found that for the same material, fatigue life prediction models depend on parameters such as stress factor, hardness, manufacturing defect, the manufacturing process itself, applied alloy heat treatment, and geometry of the element. The result of the research and analysis presents a model for determining the allowable stresses, which considers several factors such as defect area, hardness, and stress factor.

In [8], fatigue tests were analyzed under uniaxial loading of two aluminum alloys, including the 6060-T6 alloy. As a result of the tests, it was shown that the tested material is characterized by cyclic stability.

In [19], based on fatigue tests of hardened aluminum alloy 6060, the influence of initial deformation on fatigue life and the effect of aging before cyclic fatigue was determined. In addition to the determined fatigue characteristics in the stress-strain system, the resulting fatigue fractures were subjected to fractographic analysis. The proper fatigue tests were performed with the control of plastic strain amplitudes in the range $\varepsilon_{apl} = 1 \cdot 10^{-3} - 5 \cdot 10^{-3}$. For all the amplitudes used, the fatigue life of the plasticity-optimized state did not reach the fatigue life of the strain-reinforced specimens by jacking.

In [20], the mechanical properties of aluminum alloys after heat treatment were compared under the T4, T5, and T6 heat treatment methodology. It was confirmed that the maximum fatigue strength was obtained due to the use of T6 solution treatment and artificial aging.

In [41], the influence of the average stress value on the fatigue life of two aluminum alloys, including aluminum alloy 6060, was analyzed. Fatigue strength was determined for uniaxial loading with cycle asymmetry coefficient R = -1, 0, and 0.1. It has been shown that the tested material shows significant sensitivity to the influence of the average value of stresses. For tests with the cycle asymmetry coefficient R = 0 and 0.1, the fatigue life is lower by approximately—two orders of magnitude.

In the work [26], samples made of 6060 aluminum alloy friction stir welded were tested. Both mechanical and microstructural properties were tested. The research aimed to determine the optimization of the rotational speed of the tool to obtain optimal mechanical properties of the joint and the resulting microstructure.

In [24-25], a fractographic analysis of fatigue fractures of aluminum alloys after cyclic bending and torsion tests was carried out. As a result, it was found that crack propagation occurs mainly by connecting successive cracks that are formed at adjacent grain boundaries. It was found that the microstructure, type, and size of cyclic loads determine the share of trans crystalline, quasi-split, and ductile cracks, thus determining the fractography of fatigue samples.

In [34], the effect of strain location on pitting corrosion of aluminum alloy 6060 was analyzed. Focusing on deformation locations, the study shows the effect of extrusion and ECAP on the initiation and growth of pits in aluminum alloy 6060 controlling microstructural features. The source of corrosion is the cathodic behavior of the primary deposits towards the 6060 aluminum alloy. As the dissolution front approaches the next grain boundary, the decorating deposits are weakened, and the local electrochemical cell disappears. Therefore, grain clarification and sludge fragmentation increase the density of the pits but decrease the depth of the holes.

As a brief review has shown, 6060 aluminum alloy needs to be better understood in terms of fatigue in service. Therefore, this work deals with fatigue tests of this material. Only papers [20, 32, 38] analyzed the effect of heat treatment on the fatigue properties of the analyzed 6060 aluminum alloy. Besides, in the literature, there are few papers on this problem for other aluminum alloys [20, 24-25, 32]. An analysis of the influence of various treatment methods on the fatigue limit of magnesium alloy [27] can be found in the literature. Samples made using two treatment methods, T6 and T64, were accepted for analysis. This work aims to perform a fatigue test of this material in the conditions of cyclic bending, cyclic torsion, and two combinations of bending and torsion. All studies were performed with a zero mean value.

Then, a fractographic analysis was performed. On this basis, the suitability of this material for use in window and door profiles dedicated to trains can be demonstrated.

2. Material and experiment

The 6060 aluminum alloy was used for the tests. Fig. 3 shows pictures of extruded profiles used for door and window structures made of this alloy. Material for fatigue test samples was taken directly from these profiles used at the production stage.

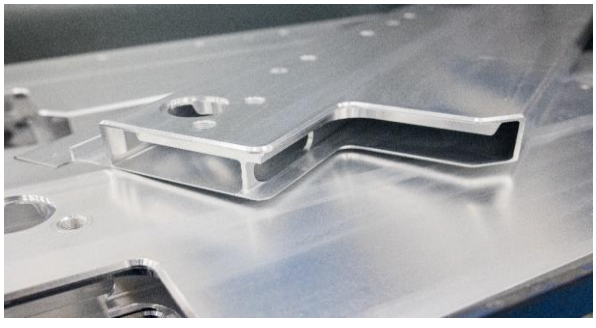

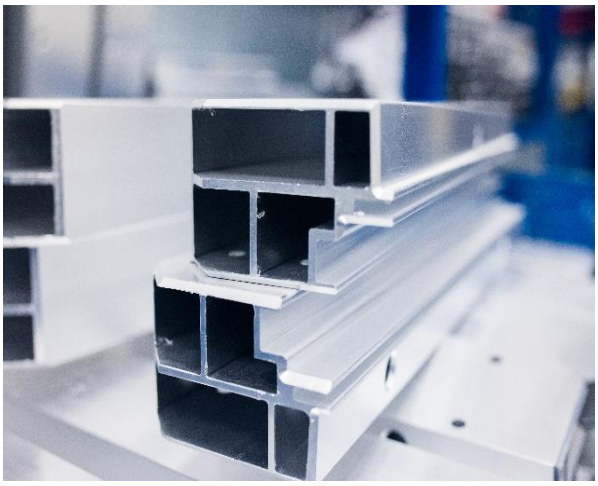

Fig. 3. Exemplary pictures of profiles from which the window and door structure of aluminum alloy 6060 is made.

For the production of windows and doors, profiles delivered directly from the manufacturers after thermal treatment are used T6 and T64 - EN 515:2017-05 [11]. The test samples were cut directly from the profiles provided to perform the experiment and calculations. The microstructure of the 6060 alloys in the T6 and T64 states is shown in Fig. 4. There are tiny points visible in the grains, which are precipitates of the strengthening phase.

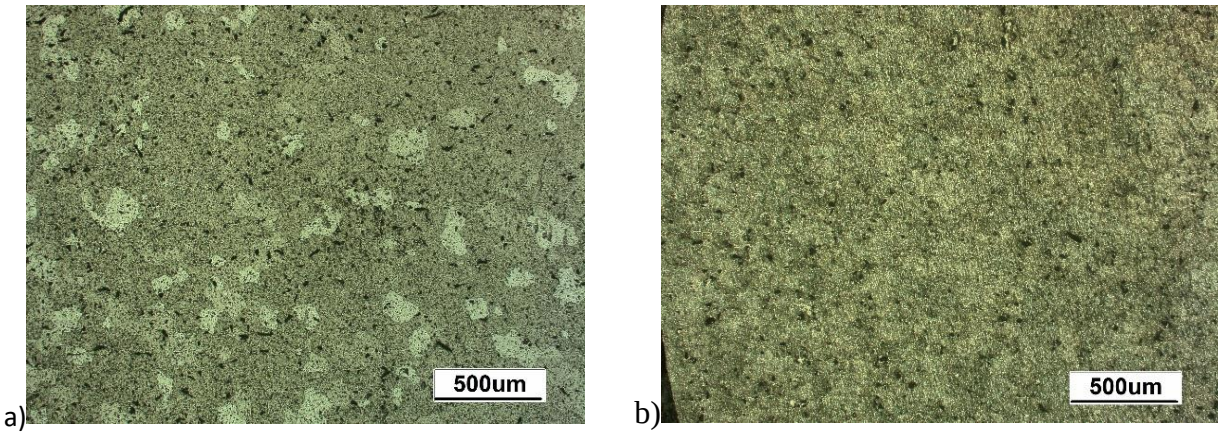

Fig. 4. Microstructure of 6060 aluminum alloy after T6 (a) and T64 (b) treatments.

The change in microstructure observed under the influence of the applied heat treatment consisted of the separation of small, numerous particles of secondary phases in the matrix, which contributed to the strengthening of the material. The largest amount of strengthening phase was obtained by using T6 treatment.

This material has various designations in the literature. Other names of aluminium 6060 are, for example, PA38, AlMgSi3.3206.

Chemical composition by the standard [12] is listed in table 1.

Table 1. Chemical composition of aluminum and aluminum alloy 6060 according to the standard EN 573-1 [12] – Al – balance.

element	Mg	Mn	Fe	Si	Cu	Zn	Cr	Ti	others
content, %	0.35-0.60	≤0.10	0.10 – 0.30	0.30 – 0.60	≤0.10	≤0.15	≤0.05	≤0.05	≤0.20

EN AW-6060 aluminum alloy has medium mechanical strength, impact strength, and good corrosion resistance. Suitable for anodizing and polishable. It has medium fatigue strength and can be machined. It is one of the better materials for door and window structures used in the railway industry. This material has different applications depending on the treatment. For T64 treatment, the alloy is characterized by increased strength and is suitable for bending. In the case of T6 treatment, high-strength elements are obtained. However, in this case, the elements are not suitable for plastic forming and bending.

Table 2 summarizes the basic properties of the material depending on the treatment used [13]. The table below shows that the profiles of aluminum alloy 60060-T64 do not meet the standard values for both plastic and temporary strengths. The data analysis in Table 2 shows that the values of the strength limit and the yield point for aluminum 6060-T64 do not reach the value of standard stresses. However, the actual values of the same alloy in the T6 state definitely exceed the standard values. Additionally, Fig. 4 shows the static tensile test charts for both treatments, and Fig. 5 shows photos of sample cracks after the static tensile test.

Table 2. Basic properties of 6060 aluminum alloy subjected to different treatment methods [13].

6060	$\sigma_{u(min)}$, MPa	σ_u, MPa	$\sigma_{y(min)}$, MPa	σ_y, MPa	$A_{50mm(min)}$, %	$A_{(min)}$, %	E, GPa
T64	180	151	120	118	12	10	69.5
T6	170	264	140	238	8	6	69.5

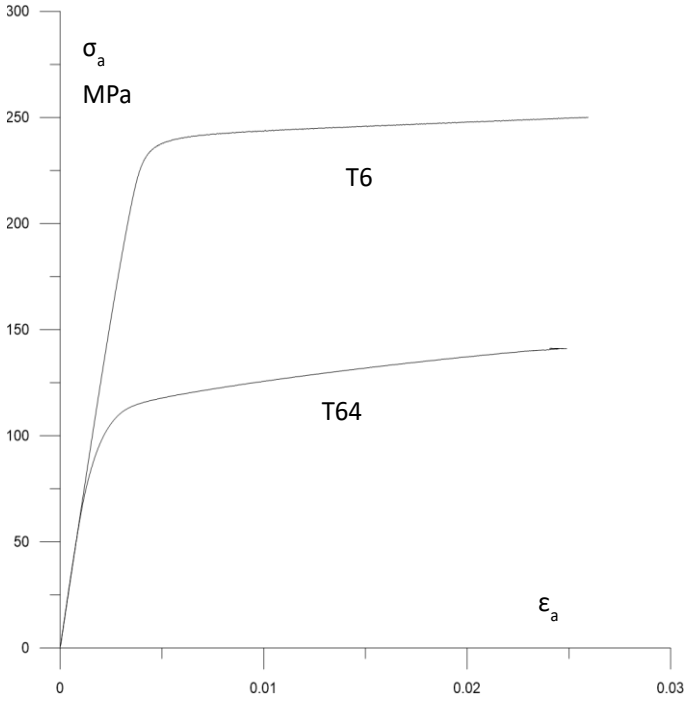

Fig. 5. Static tensile test of 6060 aluminum alloy in T64 and T6 state.

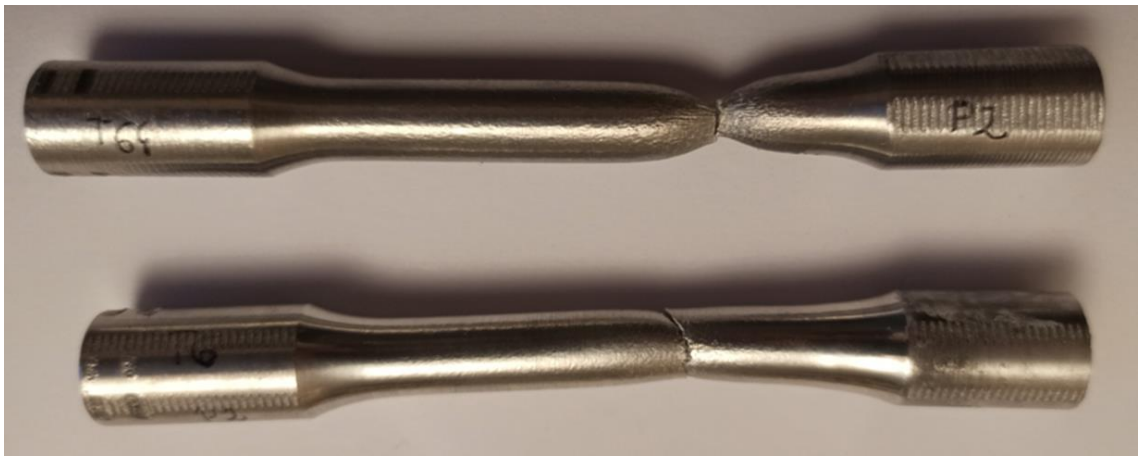

Fig. 6. Photo of samples after static tensile test in T64 and T6 state.

Most structures are subjected to complex load conditions during operation. Often, this is tension-compression with cyclic torsion or cyclic bending with cyclic torsion. With windows and doors installed in carriages, cyclic bending with additional, often significant torsion is dominant. Therefore, both cyclic bending and torsion test conditions were analyzed. Additionally, two combinations of cyclic bending and torsion were analyzed. This allows the fatigue life to be approximated for any combination of proportional cyclic bending and torsion.

Basic fatigue tests were performed on a non-standard stand designed and built at the Opole University of Technology. The research carried out at this site has been published many times by various authors—the last time it was presented in a paper [30]. A detailed description of this stand is presented in [1]. A rotating, unbalanced mass applies the fatigue load. This creates a dynamic force on the 200 mm arm. As a result, a cyclically variable torque is created in the handle. This torque, depending on the position of the head, is divided on a “diabolo” (Fig. 7) sample with a minimum diameter of 10 mm into a bending and twisting moment. As mentioned earlier, these samples were cut from the supplied profiles, and the surface in the narrowing, i.e., the critical place, was ground. As a result, normal stresses from bending and shear stresses from torsion are obtained at the critical point of the sample. The total torque controls the load on the bench. The testing frequency was constant and amounted to 29 Hz. The applied cyclic moment varied sinusoidally around the average value of 0. The head angle determined the ratio of bending to torsional moment, which resulted in various combinations of bending and torsion, from pure bending to pure torsion.

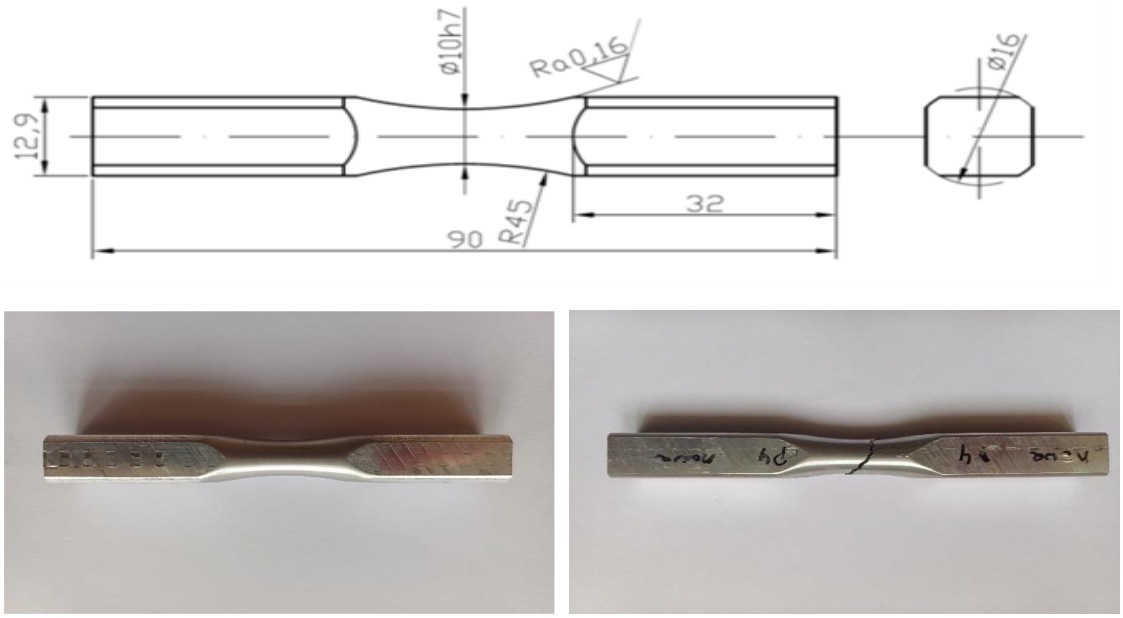

Fig. 7. Drawing and photo of the "diabolo" sample before and after the sample test.

Tables 3 and 4 show the results of fatigue tests of 6060 aluminum alloy in the T64 and T6 states, respectively. The fatigue life results are given with an accuracy of one cycle, and the stress amplitude with an accuracy of 1 MPa.

Table 3. Results of fatigue tests of aluminum alloy 6060 - T64

Bending			Torsion		
specimen	N_f, cycles	σ_a, MPa	specimen	N_f, cycles	τ_a, MPa
13	10270	183	1	2000000	61
14	47432	163	2	8474	122
15	46659	143	3	487900	92
16	1451362	102	4	668644	82
17	569643	122	5	11004386	71
18	756020	122	6	15140	102
19	21554	183	7	3700	112
20	105560	163	8	562587	82
21	118533	143	9	68884	92
22	428045	122	10	66960	102
23	2699792	102	11	19109	112
24	7551	183	12	6201	122
25	125085	142			

$\tau_a = 0.5\,\sigma_a$ $\tau_a = \sigma_a$

specimen	N_f, cycles	σ_a, MPa	specimen	N_f, cycles	σ_a, MPa
26	37388	116	39	592846	72
27	357007	101	40	268792	81
28	1661467	87	41	69495	90
29	24017	130	42	1221562	63
30	11954	145	43	6000	99
31	15000000	72	44	44788	99
32	54687	145	45	1858	108
33	16283	159	46	23766	103
35	2671	159	47	4789204	54
36	298965	116	48	3626	103
37	515132	101	49	56687	99
38	3549894	87	50	16861	90
			51	247518	81
			52	708546	72
			53	639916	63
			54	2206384	54
			55	5396843	50

Table 4. Results of fatigue tests of aluminum alloy 6060 - T6.

Bending			Torsion		
specimen	N_f, cycles	σ_a, MPa	specimen	N_f, cycles	τ_a, MPa
2	134278	183	16	98274	122
3	168380	163	17	275813	102
4	62574	204	18	124454	112
5	333998	143	19	275617	92
6	2121257	122	20	1349027	92
7	26185	224	21	227693	112
8	14314	245	23	728827	97
9	1870187	132	23	260929	107
10	294524	153	24	1740012	87
11	91075	194	25	24122	117
12	33432	214	26	40889	127
13	27833	234	27	31439	132
			28	19874	143
			29	1295223	82
			30	10560	153
			31	17413	148

$\tau_a = 0.5\,\sigma_a$ $\tau_a = \sigma_a$

specimen	N_f, cycles	σ_a, MPa	specimen	N_f, cycles	σ_a, MPa
31	30762	174	50	297290	91
32	105942	145	51	143361	100
33	324019	130	52	46049	109
34	594560	116	53	51637	118
35	87149	159	54	21574	128
36	483267	116	55	13721	137
37	20568	188	56	1857677	68
38	14504	203	57	17383	132
39	1011068	109	58	34732	123
40	446606	123	59	39910	114
41	1484083	101	60	83445	105
42	16361	195	21	173023	96
43	29901	181	62	518883	82
44	1987514	94	63	552150	73
45	156274	137	64	2935507	64
46	39230	166			

3. Fatigue life-time of 6060 aluminium alloy

Based on fatigue tests by the ASTM [3] standard, 4 fatigue characteristics were determined for individual load conditions and treatment methods.

For T64 treatment, the following characteristics are obtained:

Cyclic bending

$$\sigma_a = 503.81 N_f^{-0.110} \quad (1)$$

Cyclic torsion

$$\tau_a = 230.61 N_f^{-0.078} \quad (2)$$

Cyclic bending with torsion

$$\sigma_a = 2\tau_a = 358.62 N_f^{-0.096} \quad (3)$$

and

$$\sigma_a = \tau_a = 249.85 N_f^{-0.097} \quad (4)$$

In contrast, for T6 treatment, the following values were obtained:

Cyclic bending

$$\sigma_a = 941.27 N_f^{-0.141} \quad (5)$$

Cyclic torsion

$$\tau_a = 408.18 N_f^{-0.109} \quad (6)$$

Cyclic bending with torsion

$$\sigma_a = 2\tau_a = 807.66 N_f^{-0.146} \quad (7)$$

and

$$\sigma_a = \tau_a = 539.77 N_f^{-0.144} \quad (8)$$

Figs. 8 and 9 show the obtained fatigue characteristics and the experimental points. The comparison of fatigue characteristics shows that they are practically parallel. In the case of aluminum after T64 treatment, the slope of the characteristics reaches a value in the range of 0.096-0.110 according to formulas (1), (3), and (4), and for torsion it is a smaller value equal to 0.078 - Eg. (2). Similarly, in the case of aluminum after T6 treatment, the inclination of the characteristics reaches a value in the range of 0.141-0.146 according to formulas (5), (7) and (8), and for torsion it is a smaller value equal to 0.109 - Eg. (6). The best way to assess the fit of fatigue characteristics to the obtained experimental results is to determine the Coefficient of determination, R-squared (R^2). Table 5.0 lists these values for individual test combinations and the T64 and T6 treatments used. The analysis of the obtained calculation results shows that the Coefficient of determination is high and ranges from 0.841 to 0.991. For both treatments, the smallest is for cyclic twisting. The average value of the R^2 coefficient for all studies is 0.992. It should be noted that for T6 machining, this coefficient is much higher (0.956) compared to T64 machining (0.889). This is probably because it is more difficult to achieve the desired roughness for material after T64 processing, and, as a result, larger scatters are obtained. The largest deviation from non-parallelism was obtained for cyclic torsion (T64 and T6 treatment) in relation to other load conditions. In the case of cyclic torsion, a fatigue crack may appear at any point on the periphery because, at each point on the perimeter, there are tangential stresses of the same value. In other cases, however, only two points are on the perimeter. Therefore, in addition to the scale effect [7, 9], we also have the number of samples effect [4, 33] or the weakest link effect [5-6].

Table 5. Coefficient of determination, R-squared (R^2) for individual tests and applied treatments.

	$\tau_a = 0.$	$\tau_a = 0.5\,\sigma_a$	$\tau_a = \sigma_a$	$\sigma_a = 0$	Mean value
T64	0.924	0.914	0.877	0.841	0.889
T6	0.958	0.991	0.978	0.898	0.956
Mean value	0.941	0.952	0.927	0.869	0.992

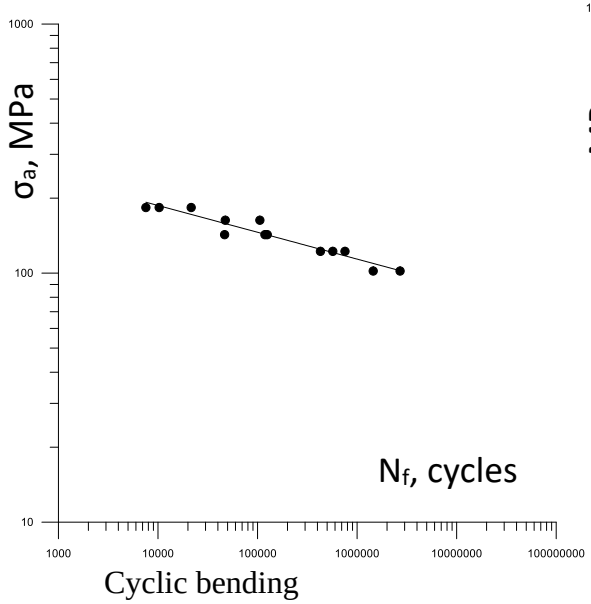

Cyclic bending

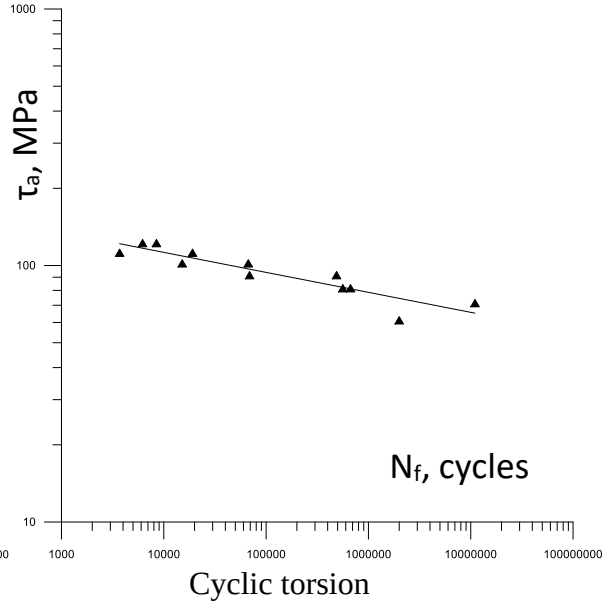

Cyclic torsion

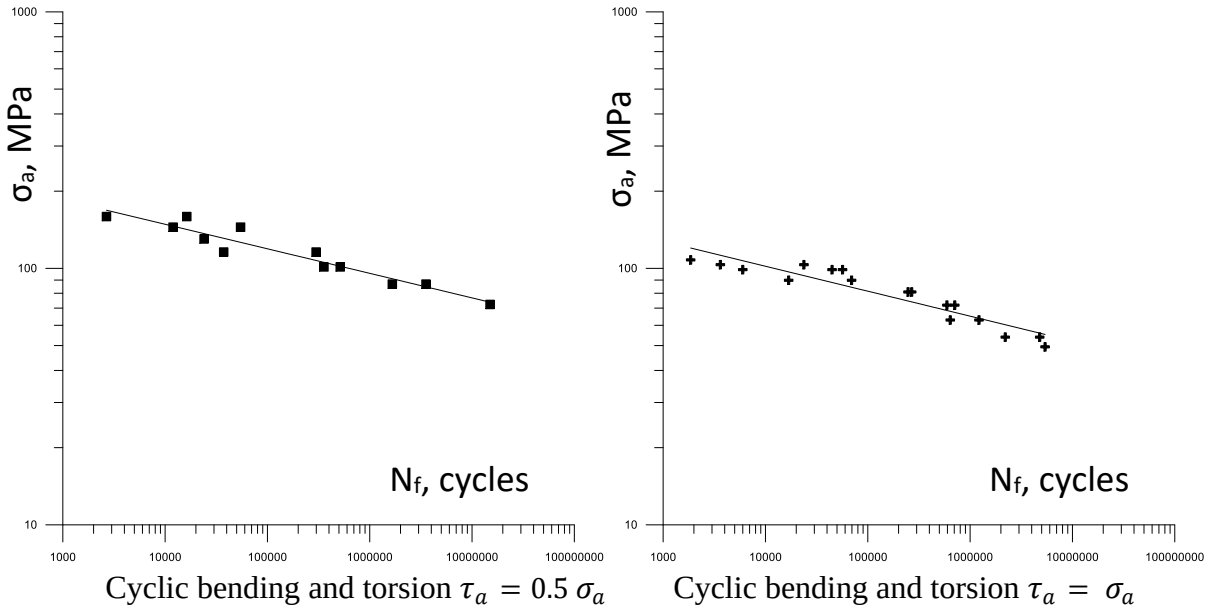

Fig. 8. Fatigue characteristics for individual combinations of fatigue tests of aluminum alloy 6060-T64 with marked experimental points.

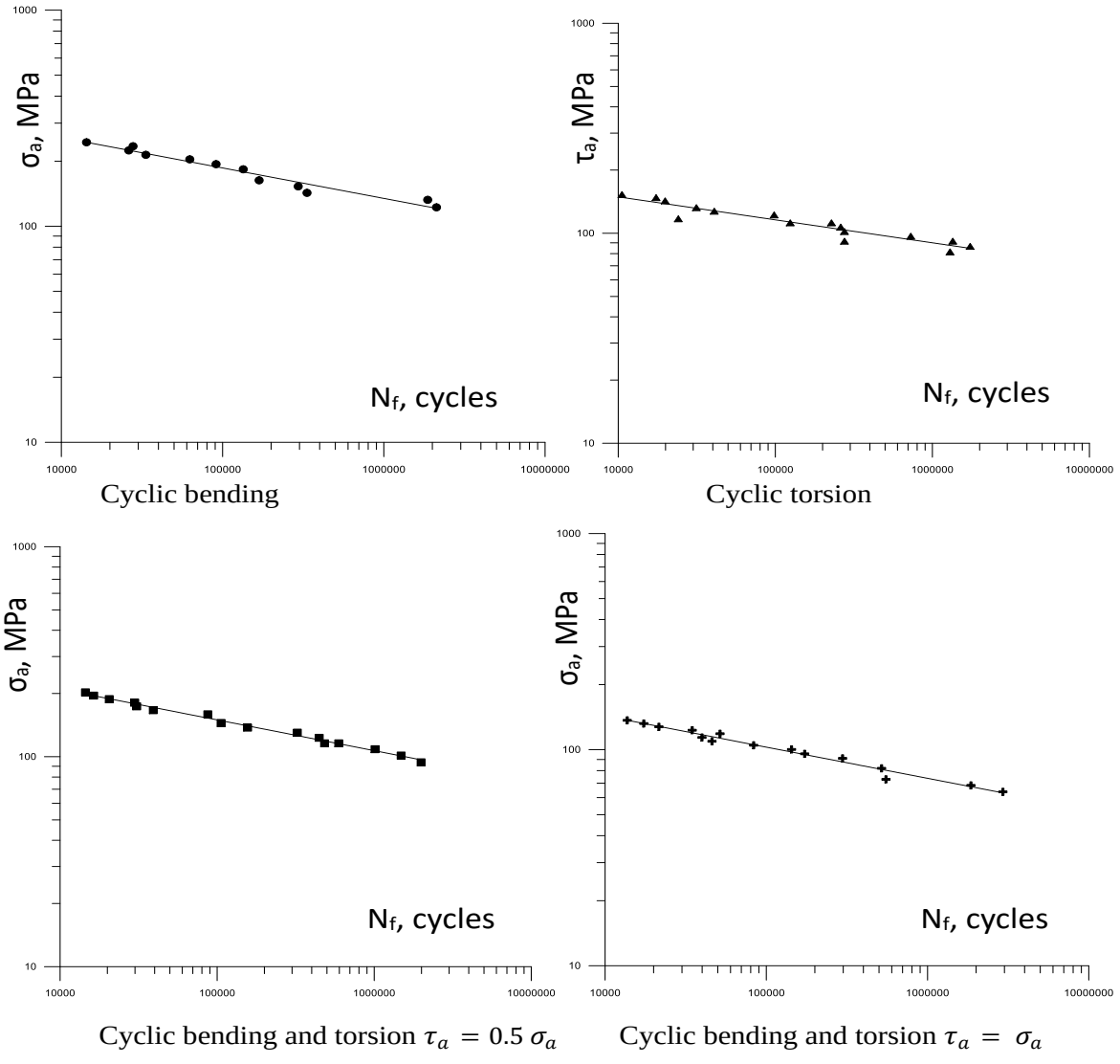

Fig. 9. Fatigue characteristics for individual combinations of fatigue tests of aluminum alloy 6060-T6 with marked experimental points.

Fig. 10 presents the fatigue characteristics to compare the applied treatment methods for individual loads. These drawings indicate durability $N_f = 10^5$ cycles. For this fatigue life, as values from the middle part of the determined characteristics, stress amplitudes were used for further analysis.

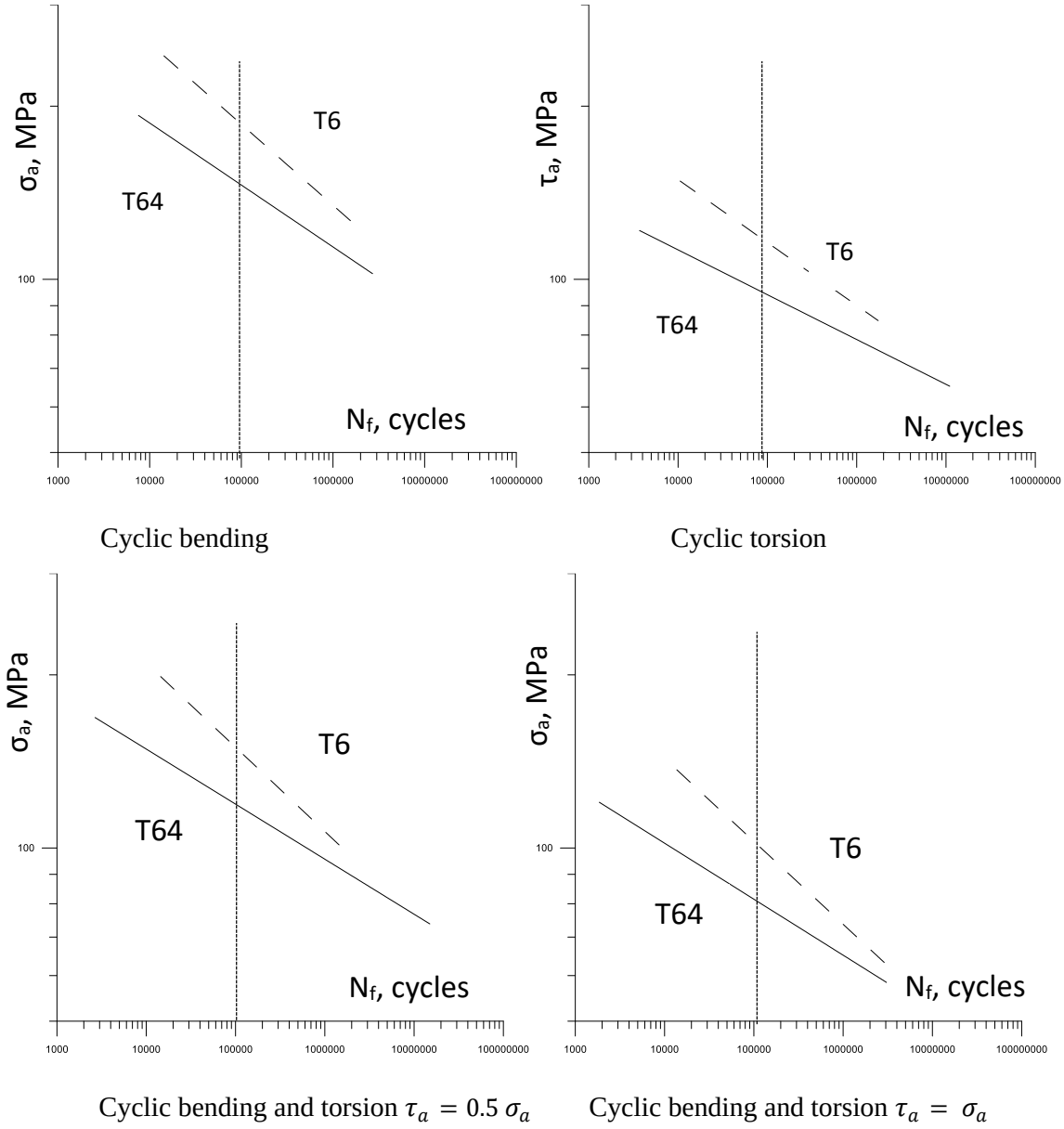

Fig. 10. Comparison of fatigue characteristics of 6060 aluminum alloy in T64 and T6 state for individual combinations of fatigue tests.

Fatigue tests for a combination of cyclic proportional bending and torsion are most often and easiest described by the Gough-Pollard criterion [18] in the formula

$$\sigma_{aeq} = \sqrt{\sigma_a^2 + \left(\frac{\sigma_{a-1}(N_f)}{\tau_{a-1}(N_f)}\tau_a\right)^2}, \qquad (9)$$

where:

σ_{a-1} (Nf) - normal stress amplitude for cyclic in plane bending for a given number of cycles, τ_{a-1} (N_f) - shear stress amplitude for cyclic torsion for a given number of cycles.

Fig. 11 presents the Gough-Pollard criterion for the conducted fatigue tests of the 6060 aluminum alloy subjected to the T64 and T6 treatment method, together with the marked stress values σ_{a-1} (N_f) and τ_{a-1} (N_f) for individual stress states, as mentioned earlier, for $N_f = 10^5$ cycles. From the analysis of the figure, it is visible that in the case of the combination of $\tau_a = 0.5\,\sigma_a$ and $\tau_a = \sigma_a$ of proportional bending with torsion, the values determined experimentally are each time higher than those resulting from the description of the fatigue process using the criterion (9). For fatigue life, this increase is $N_f = 10^5$ cycles,

30% for bending and 23% for torsion. For other fatigue strengths from 10,000 to 1,000,000 cycles, after calculation data presented in Figs. 8-10, the tested alloy in the case of T6 treatment is also characterized by higher fatigue strength compared to T64 treatment, from 40 to 22% for fatigue life in case of bending (Eqs. (1) and (5)), and analogously from 34 to 15% for torsion (Eqs. (2) and (6)). In case of extrapolation of fatigue characteristics beyond the scope of fatigue tests, for greater durability (>100,000,000), treatment of 6060 aluminum alloy is practically irrelevant. On the other hand, for small durability, the treatment has a significant impact on the fatigue strength.

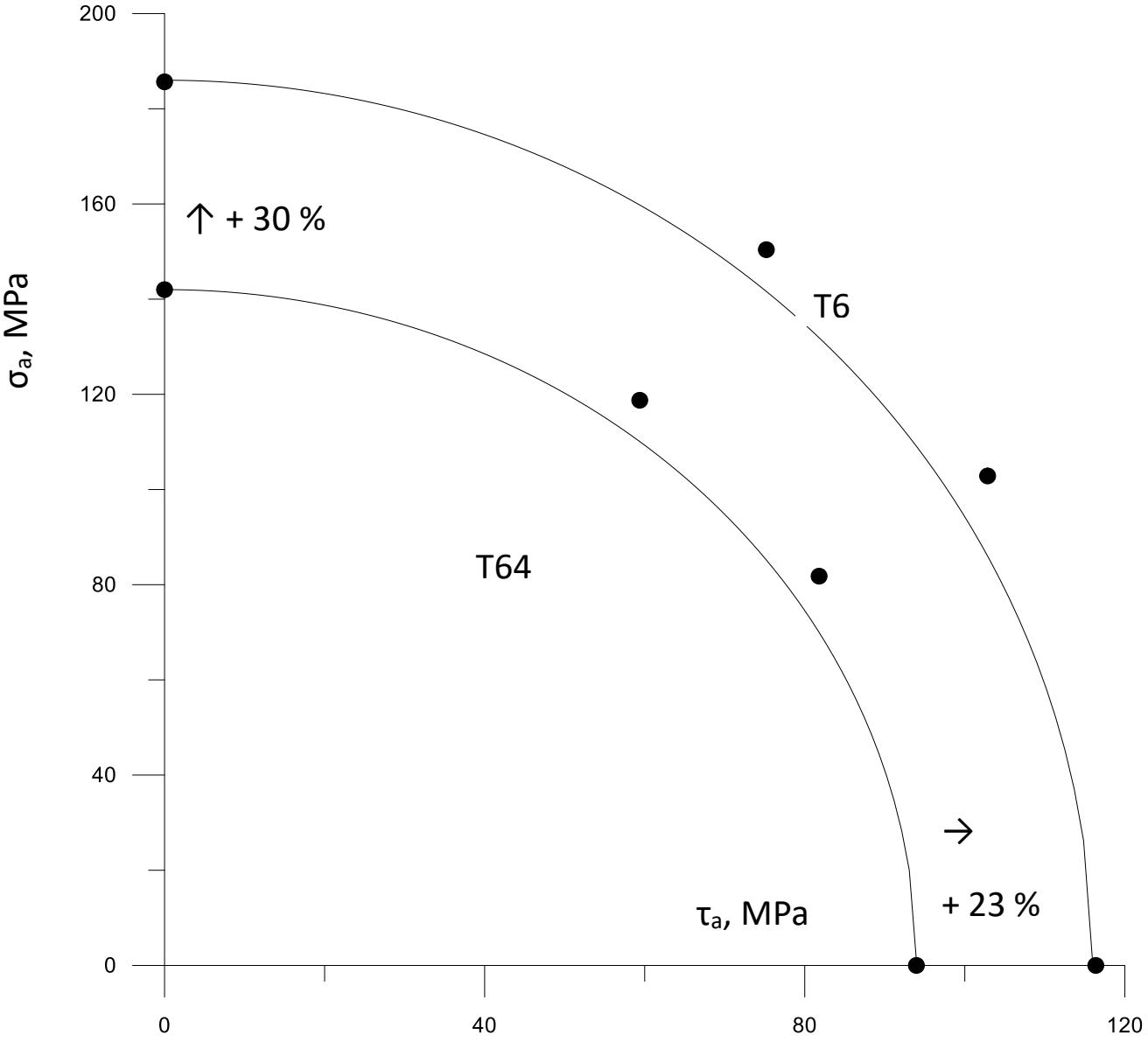

Fig. 11. Gough-Pollard characteristics for fatigue tests of aluminum alloy 6060 in the T64 and T6 treatment state with marked stress values for individual stress states for $N_f = 10^5$ cycles.

4. Fractography

The fracture images were observed using a high-performance Tescan Vega 4 Scanning Electron Microscope with a tungsten filament, operated at 20 kV in low-vacuum mode to prevent sample charging. The microscope is equipped with a secondary electron (SE) detector, which will allow to obtain topographic images of the surface of the samples. A fairly large range of magnifications, a large depth of focus, and a high resolving power of the SEM microscope, together with the possibility of continuous observation of the fracture surface at gradually increasing magnifications, enable observation of the characteristic features of crack surfaces. The specimens for SEM analysis were cleaned by using an ultrasonic cleaning which eliminates any foreign material.

Fractography of fatigue fractures for the alloy after T64 treatment is shown in Figs. 12-19, where Figs. 12-13 show the surface obtained from cyclic bending, Figs. 14-15 from torsion, Figs. 16-17 from the combination of bending and torsion $\tau_a=0.5\sigma_a$, and Figs. 18-19 for combinations $\tau_a=\sigma_a$.

In the case of bending (Figs. 12-13), all fractures are characterized by the presence of fatigue zones with clearly marked fatigue lines defining the direction of crack development and the presence of residual zones in the vicinity of the bending plane. Such fractures are characteristic of samples heavily loaded during bending, which also occurs for a less loaded sample (Fig. 13).

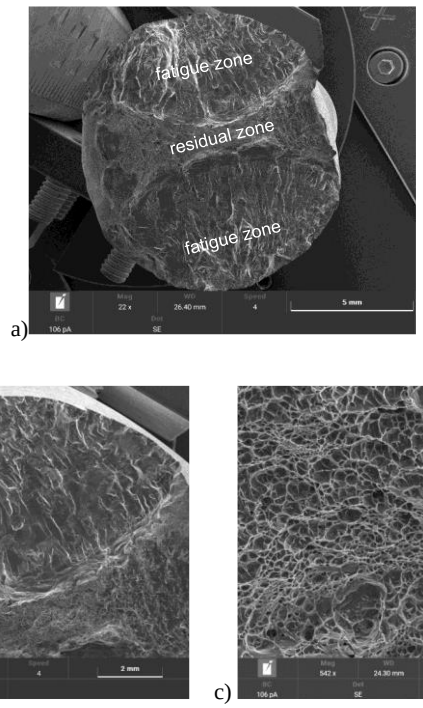

Fig. 12. Fatigue fracture of the alloy after T64 treatment caused by bending:a) fracture morphology, b) surface in the area of the fatigue zone,c) surface in the area of the residual zone(specimen 13 - 10,270 cycles).

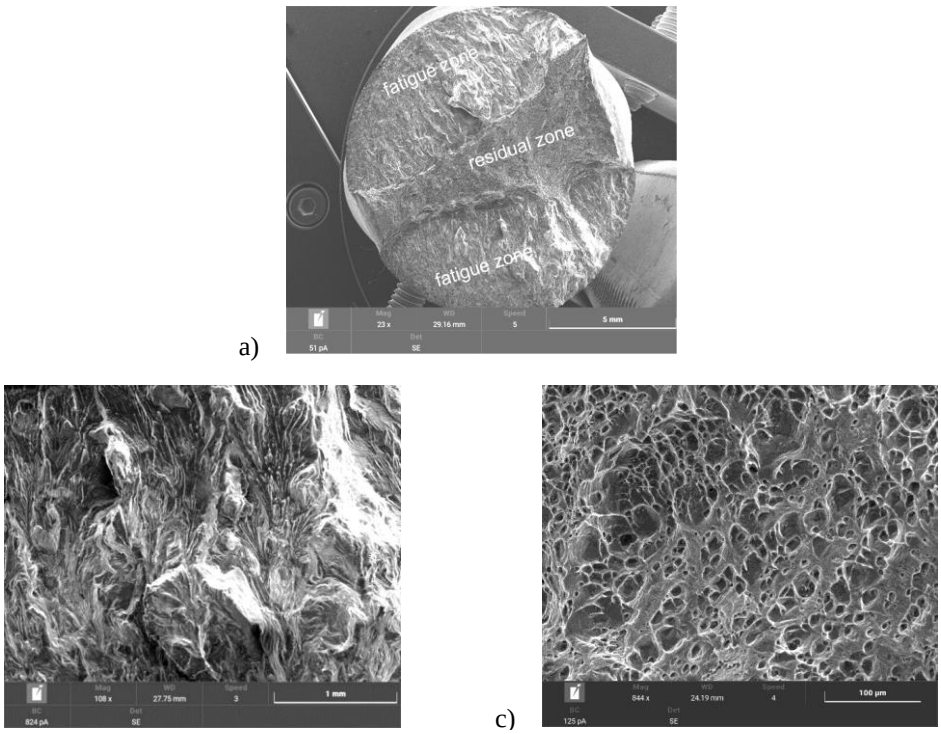

Fig. 13. Fatigue fracture of the alloy after T64 treatment caused by bending:a) fracture morphology, b) surface in the area of the fatigue zone, c) surface in the area of the residual zone (specimen 23 – 2 699792 cycles).

In the case of torsion (Fig. 14), the occurrence of an oval fatigue zone on the cross-section initiated from one focus and a fatigue zone resulting from rapid decohesion of the material is characteristic. A slightly different character, although caused by the same cause, has a fracture presented in Fig. 15. Fatigue cracks started simultaneously in many foci around the circumference, hence the high density of focal faults. In this case, we are dealing with a strong load, and the cracks developed proportionally from the sample's surface, where the same state of stress was present.

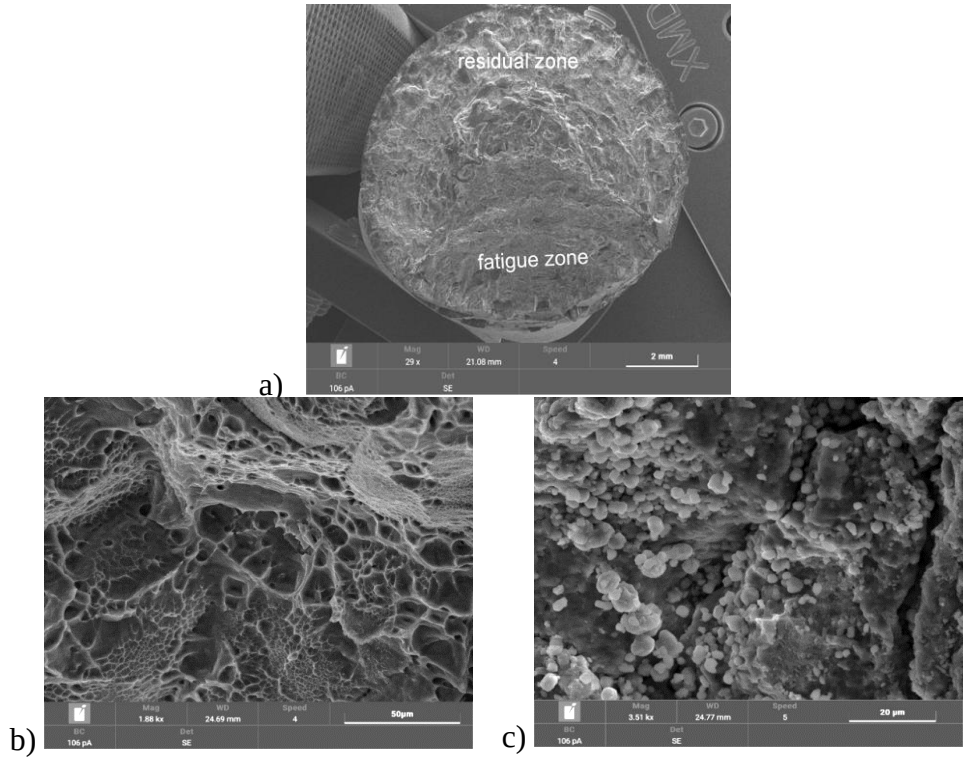

Fig. 14. Fatigue fracture of the alloy after T64 treatment caused by torsion: a) fracture morphology, b) surface in the area of the fatigue zone,c) surface in the area of the residual zone (specimen 5 – 11 004 384 cycles).

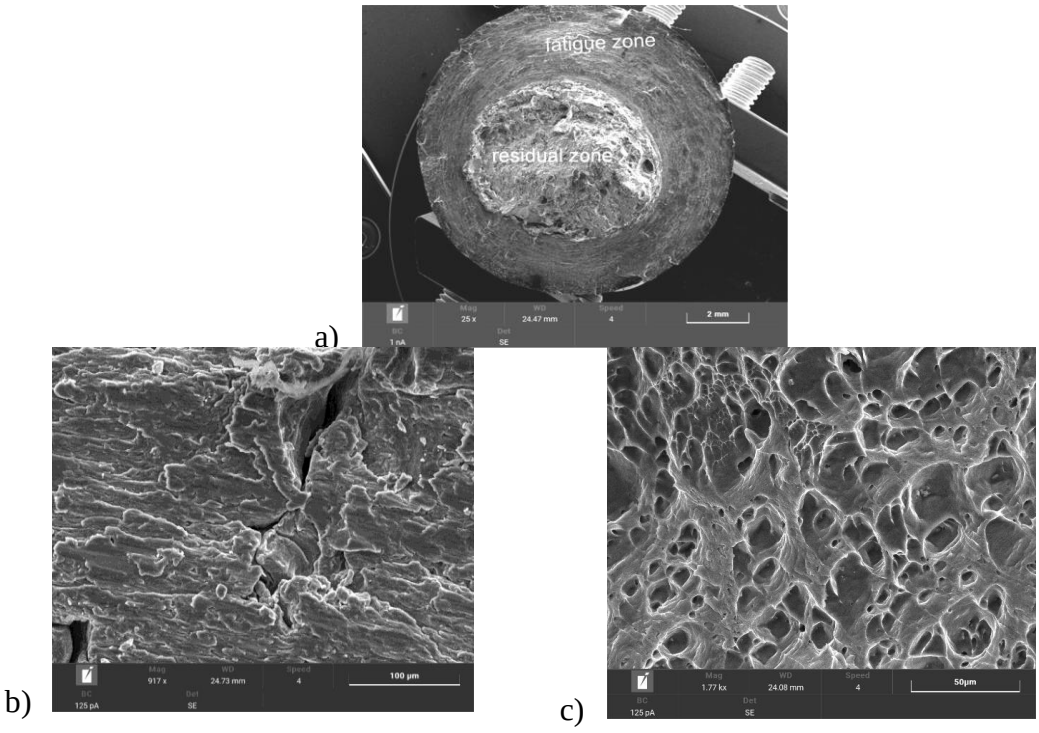

Fig. 15. Fatigue fracture of the alloy after T64 treatment caused by torsion: a) fracture morphology, b) surface in the area of the fatigue zone,c) surface in the area of the residual zone(specimen 7 – 3 700 cycles)

In the case of the combination of bending and torsion, both for $\tau_a=0.5\sigma_a$ (Figs. 16-17) and $\tau_a=\sigma_a$ (Figs. 18-19), bands of successive depressions and bulges are visible, i.e., fatigue bands of a plastic property running parallel to the crack face. The striations are continuous and regular, a trace of a crack moving in each cycle, but they do not cover the entire surface of the scrap. Especially in the case of heavily loaded samples, fatigue bands can be clearly seen for both analyzed combinations of bending and torsion.

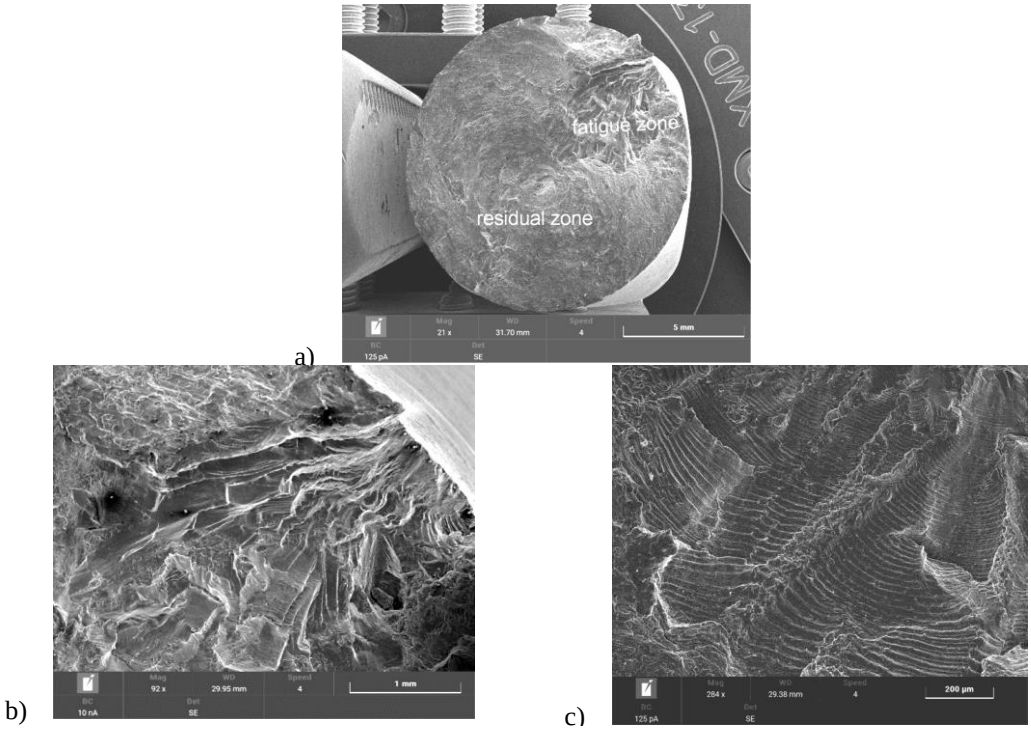

Fig. 16. Fatigue fracture of the alloy after T64 treatment caused by combination of bending and torsion τa=0.5σaa) fracture morphology, b-c) fatigue bands in the fatigue zone (specimen 35 – 2671 cycles).

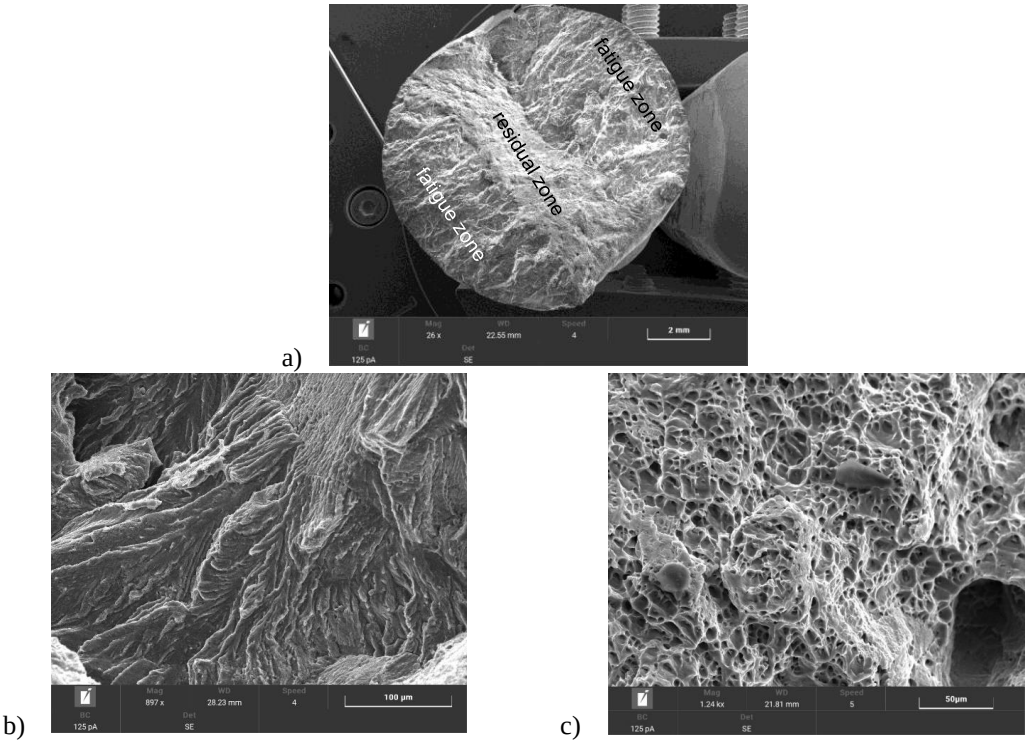

Fig. 17. Fatigue fracture of the alloy after T64 treatment caused by combination of bending and torsion τa=0.5σaa) fracture morphology, b) fatigue bands in the fatigue zone,c) surface in the area of the residual zone (specimen 38 – 3 549 894 cycles).

a)

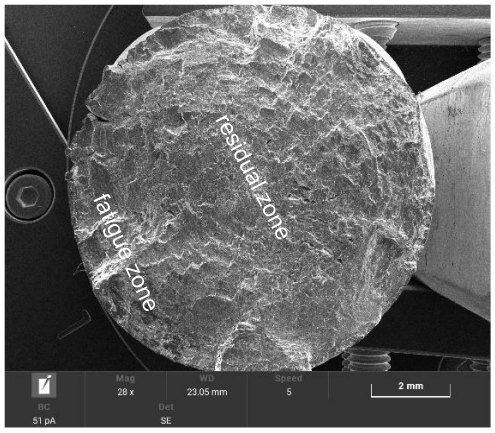

b)

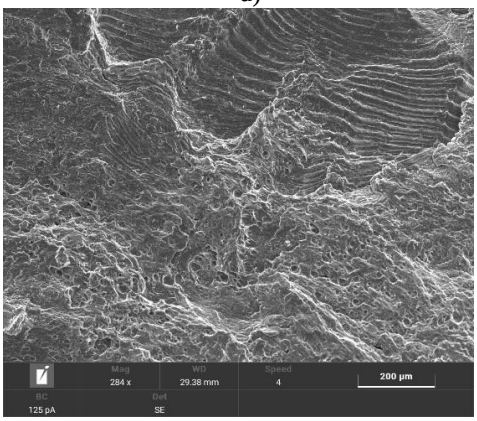

c)

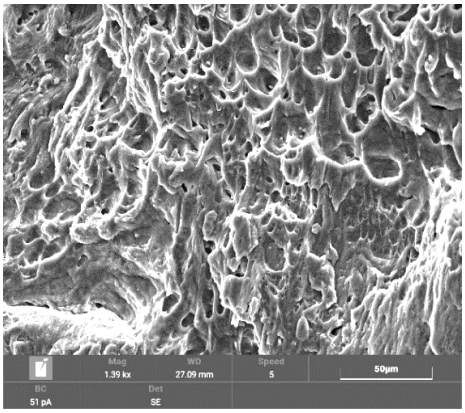

Fig. 18. Fatigue fracture of the alloy after T64 treatment caused by combination of bending and torsion $\tau_a=\sigma_a$, a) fracture morphology, b) fatigue bands in the fatigue zone, c) surface in the area of the residual zone (specimen 44 – 44 788 cycles).

a)

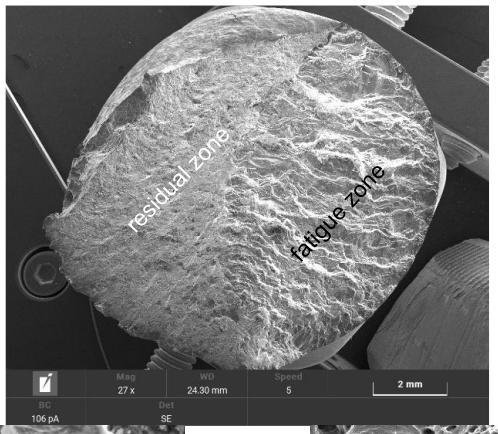

b)

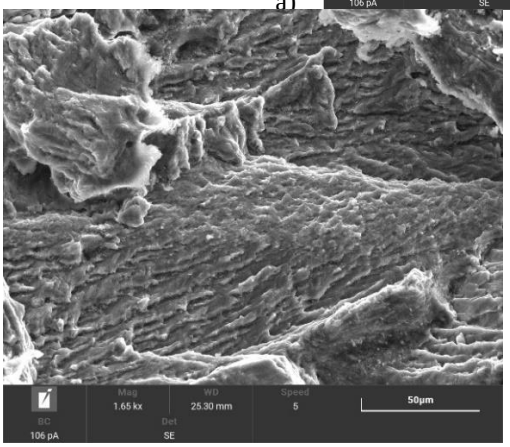

c)

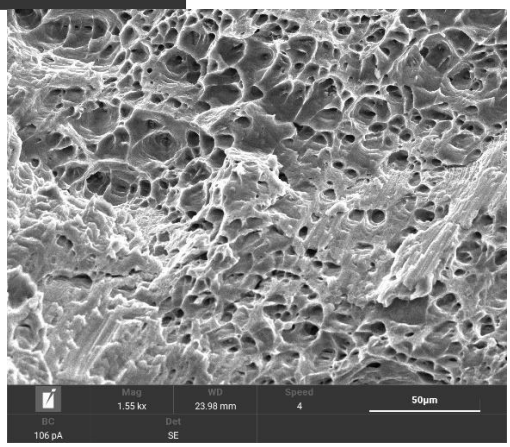

Fig. 19. Fatigue fracture of the alloy after T64 treatment caused by combination of bending and torsion $\tau a=\sigma a$, a) fracture morphology, b) fatigue bands in the fatigue zone,c) surface in the area of the residual zone (specimen 54 – 2 206 384 cycles).

In the case of bending, a similar arrangement of fracture surfaces was observed for the T6-treated alloy as for the T64-treated alloy (Figs. 20-21). A fatigue zone is visible, characterized by fatigue lines and a residual zone with a honeycomb structure (characteristic dimples of various sizes). The formation of fatigue lines can be attributed to plastic deformations occurring at the crack front due to a change in the load direction. In both cases, two fatigue zones are noticeable, lying opposite in relation to the neutral bending plane, which develops from the crack surface. When the surface load is higher, fatigue cracks are slightly more pronounced.

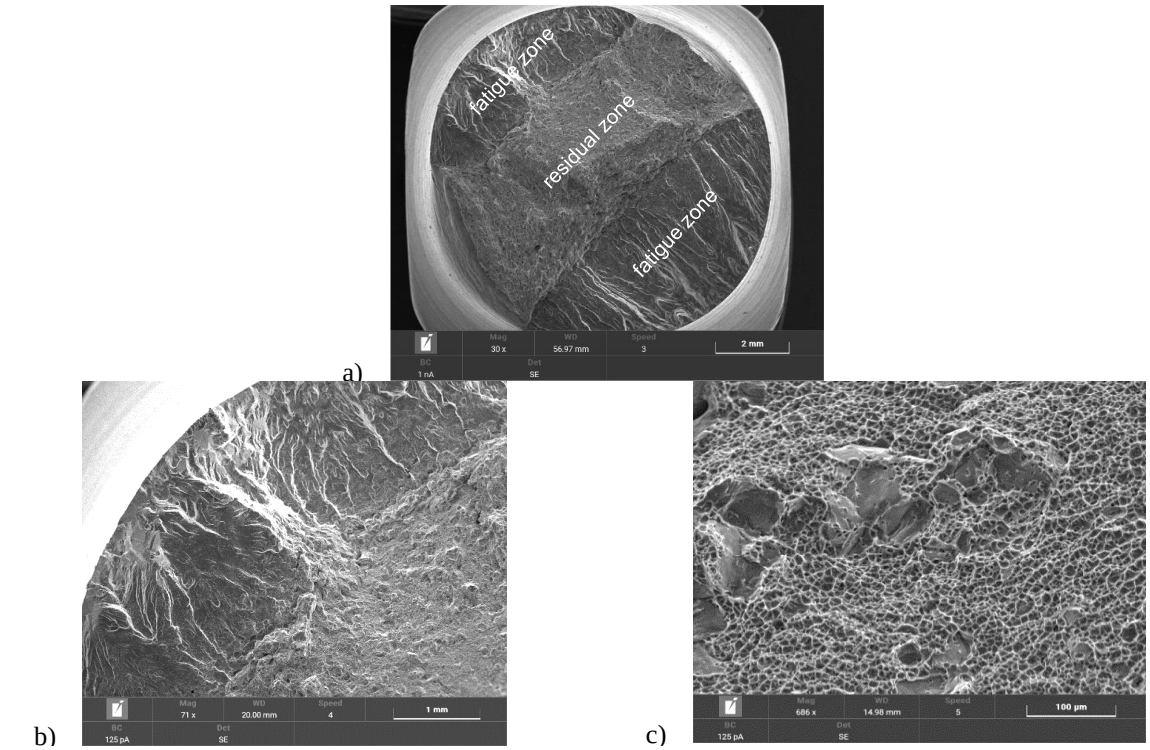

Fig. 20. Fatigue fracture of the alloy after T6 treatment caused by bending, a) fracture morphology, b) surface in the area of the fatigue zone,c) surface in the area of the residual zone (specimen 8 –14 314 cycles).

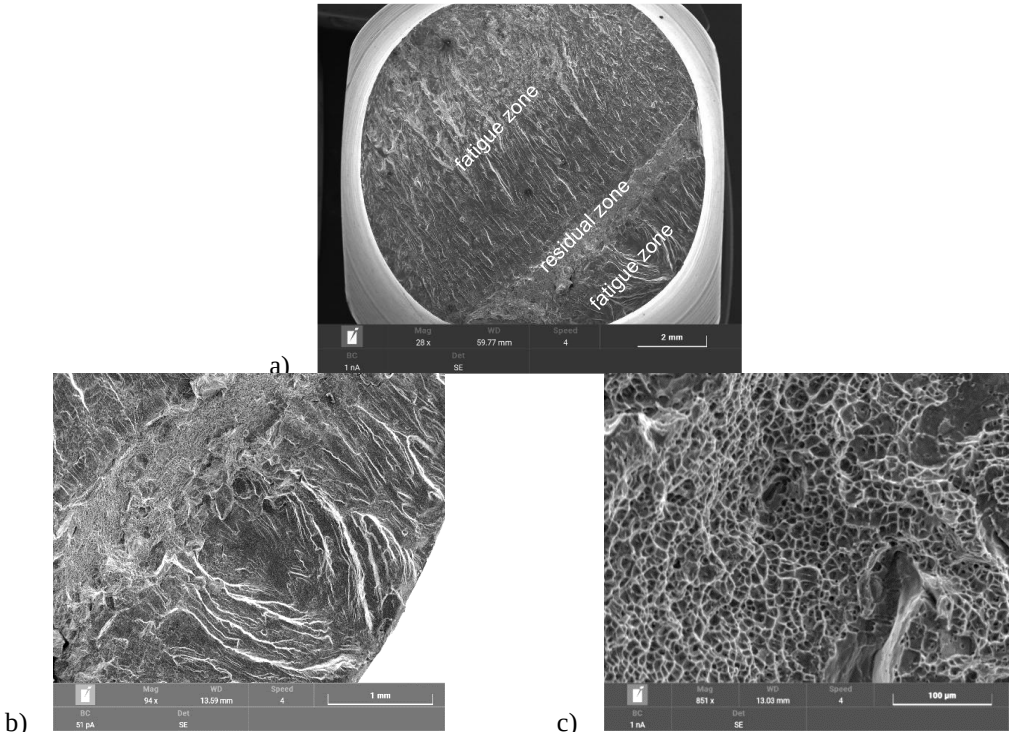

Fig. 21. Fatigue fracture of the alloy after T6 treatment caused by bending, a) fracture morphology, b) surface in the area of the fatigue zone,c) surface in the area of the residual zone(specimen 9 - 1 870 187 cycles)

In the case of torsion (Figs. 22-23), the lack of fatigue lines is characteristic. Similar observations were made for twisted alloy samples after T64 treatment. In the case of a higher load, it is noticeable that the initiation of fatigue cracks occurred on ¾ of the circumference. It should be recalled that for the T64 state, it was the entire circuit.

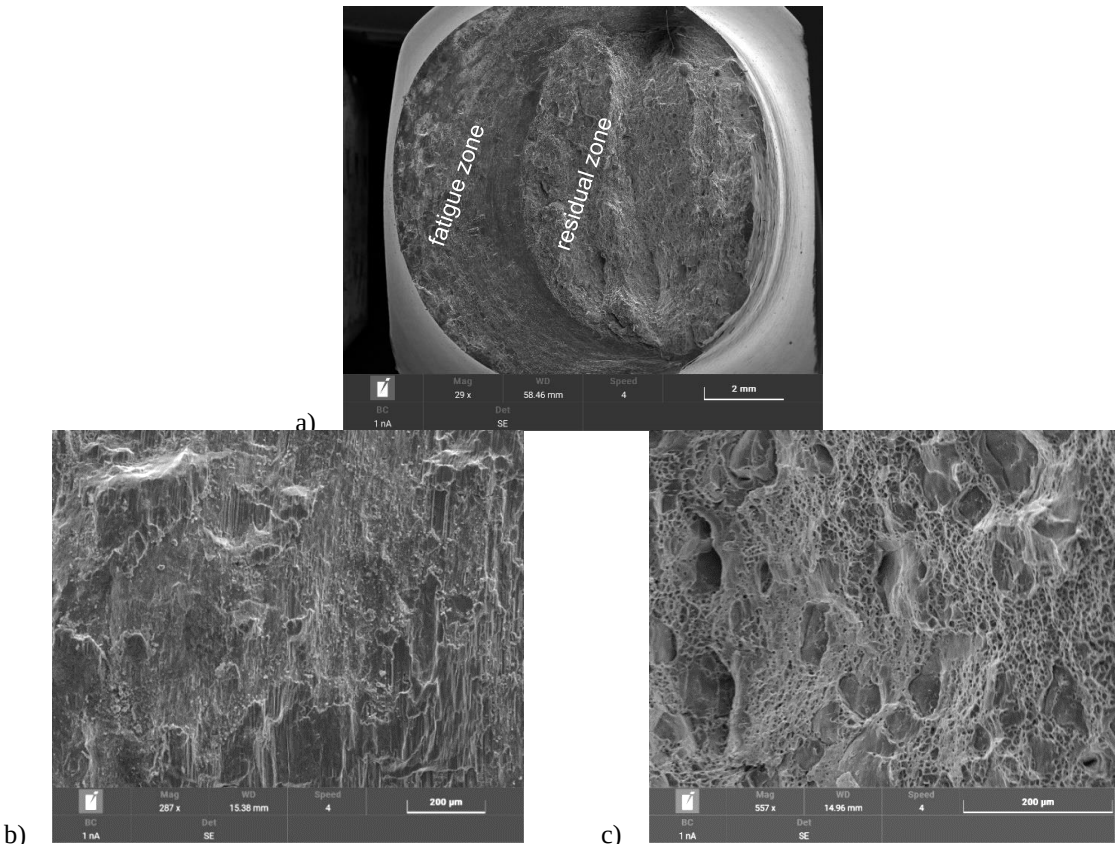

Fig. 22. Fatigue fracture of the alloy after T6 treatment caused by torsion, a) fracture morphology, b) surface in the area of the fatigue zone, c) surface in the area of the residual zone (specimen 25 –24 122 cycles).

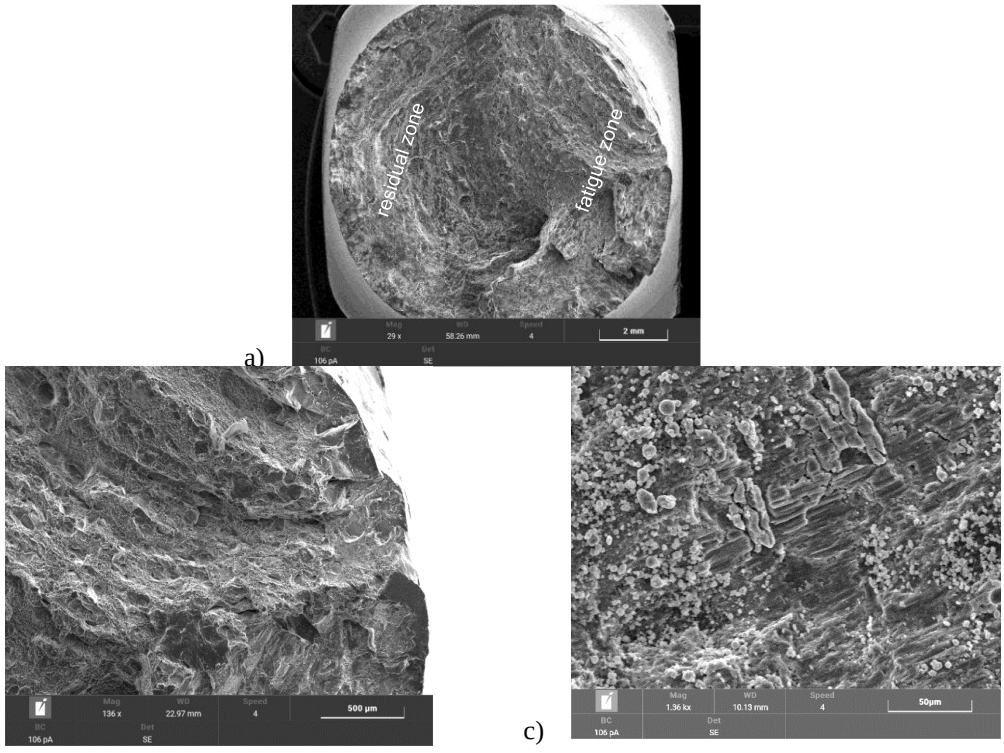

Fig. 23. Fatigue fracture of the alloy after T6 treatment caused by torsion, fracture morphology, b) surface in the area of the fatigue zone, c) surface in the area of the residual zone (specimen 20 –1 349 027 cycles).

The surface of the fractures looks completely different for the combination of bending and torsion (both for the combination of bending and torsion $\tau_a=0.5\sigma_a$ and $\tau_a=\sigma_a$) of the alloy subjected to T6 treatment method (Figs. 24-27). Here, in principle, it is possible to distinguish a characteristic structure of the fractures in the same way as for bending samples (both after T6 and T64 treatment). In this situation, the plastic property of fatigue scraps is evidenced by the presence of numerous depressions and furrows on the surface of the crack, visible in the SEM microscope at higher magnifications. In this case, as before, the fatigue zone is more pronounced when a greater load is applied.

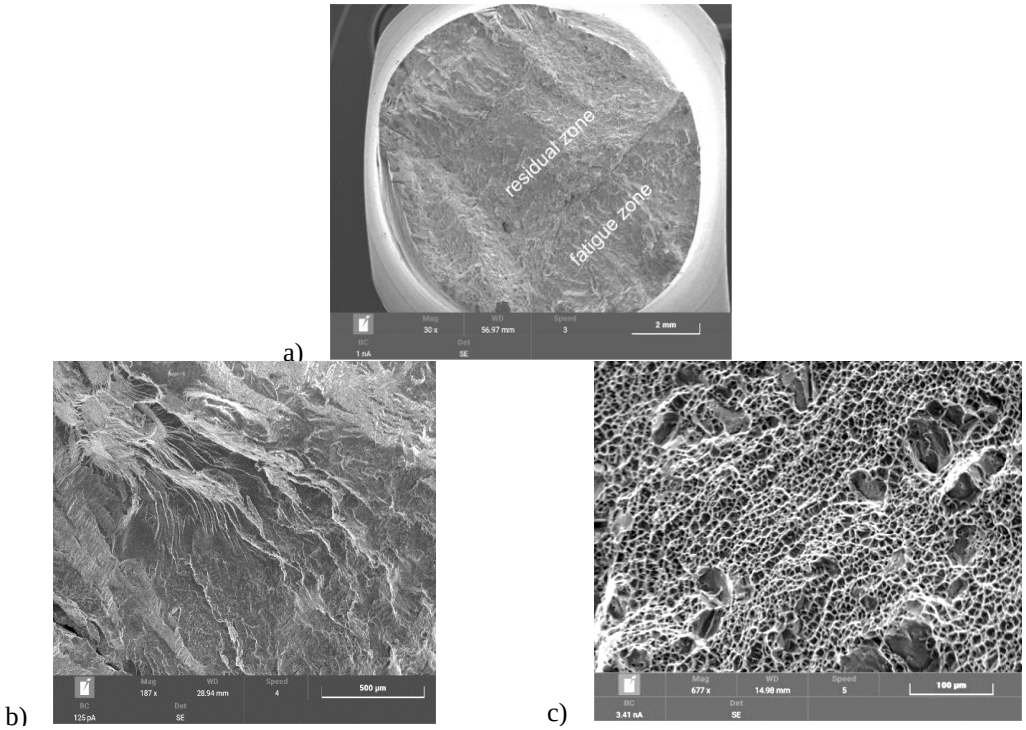

Fig. 24. Fatigue fracture of the alloy after T6 treatment caused by combination of bending and twisting τa=0.5σa, a) fracture morphology, b) surface in the area of the fatigue zone,c) surface in the area of the residual zone (specimen 38 –14 504 cycles).

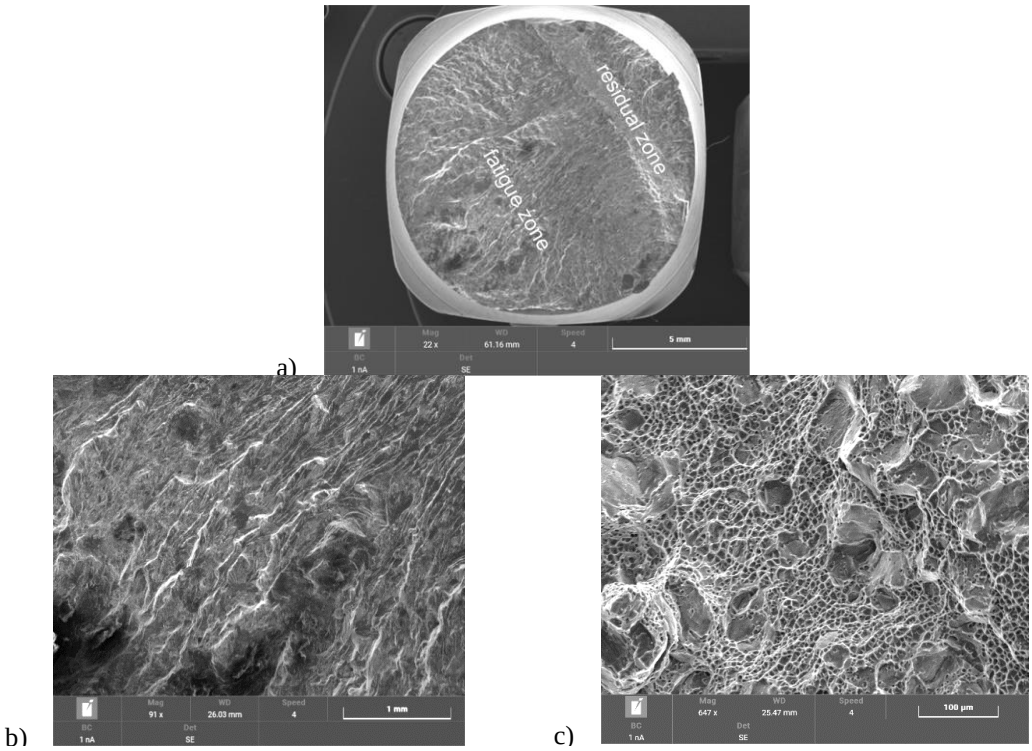

Fig. 25. Fatigue fracture of the alloy after T64 treatment caused by combination of bending and twisting τa=0.5σa, a) fracture morphology, b) surface in the area of the fatigue zone,c) surface in the area of the residual zone (specimen 44 - 1 987 514 cycles).

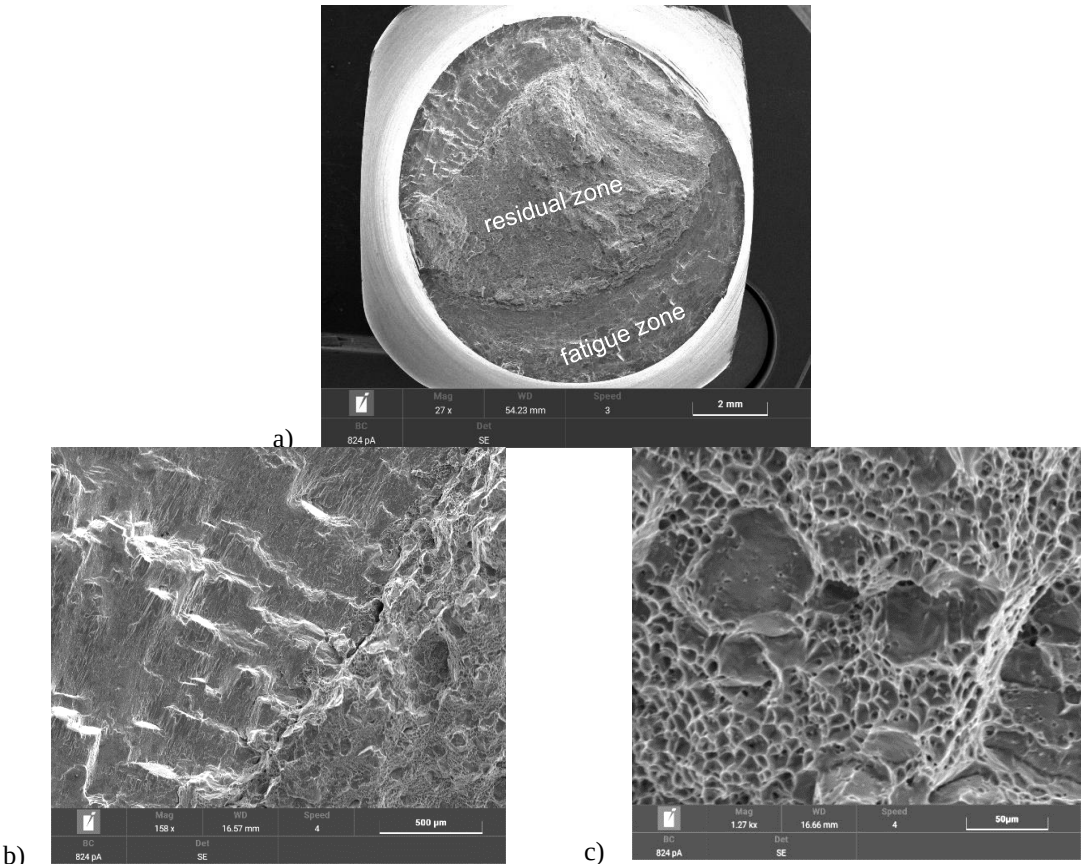

Fig. 26. Fatigue fracture of the alloy after T64 treatment caused by combination of bending and torsion τa=σa. a) fracture morphology, b) surface in the area of the fatigue zone,c) surface in the area of the residual zone (specimen 55 –13 721 cycles).

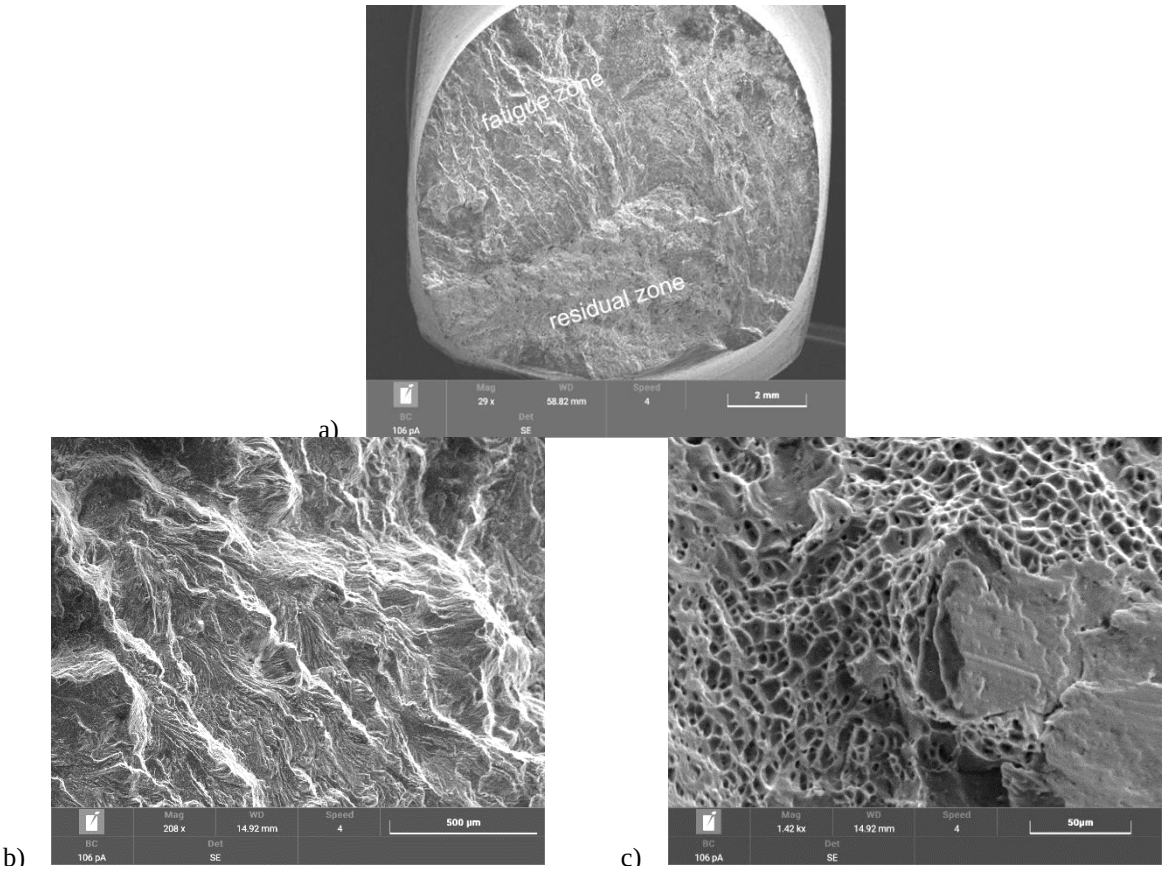

Fig. 27. Fatigue fracture of the alloy after T64 treatment caused by combination of bending and torsion $\tau_a=\sigma_a$, a) fracture morphology, b) surface in the area of the fatigue zone,c) surface in the area of the residual zone (specimen 64 -2 935 507 cycles).

Table 5. Fatigue characteristics.

Type of applied load	T64	T6
Cyclic bending	• fatigue zone with clearly marked fatigue lines residual zone near the bending plane	• fatigue zone with clearly marked fatigue lines • residual zone with a honeycomb structure
Cyclic torsion	• oval fatigue zone • no fatigue lines	• no fatigue lines
Cyclic bending with torsion $\tau_a=0.5\sigma_a$	• fatigue stripes of an artistic property	• pits and grooves on the crack surface
Cyclic bending with torsion $\tau_a=\sigma_a$		

Table 5 lists the characteristic features of fatigue fractures obtained for the samples of the analyzed material for the T6 and T64 states

5. Conclusions

From the conducted static, fatigue, and fractographic analyses, it can be concluded that:

1. The 6060 aluminum alloy differs in static strength depending on the treatments. For T6 treatment, the tensile strength is 264 MPa, and for T64, 151 MPa. Similarly, in the case of the yield point, this strength is 238 MPa and 118 MPa, respectively.
2. In case of extrapolation of fatigue characteristics beyond the scope of fatigue tests, for greater durability (>100,000,000), treatment of 6060 aluminum alloy is practically irrelevant. On the other hand, for small durability, the treatment has a significant impact on fatigue strength.
3. In the case of T6 treatment, the tested alloy is characterized by a higher fatigue strength than T64 treatment, from 40 to 22% for fatigue life from 10,000 to 1,000,000 cycles in the case of bending and analogically from 34 to 15% in torsion.
4. Fatigue characteristics for individual load combinations for both considered flashings (T64 and T6) are practically parallel. The greatest deviation from this parallelism is characterized by cyclic torsion.
5. Fractographic studies of the cracking mechanism showed that fatigue cracking, regardless of the applied heat treatment, has a plastic character. In the case of bending and a combination of bending and torsion, this is evidenced by visible plastic fatigue stripes, which are macroscopic symptoms of fatigue scrap. In the case of torsion, the absence of such stripes may indicate a steady and continuous operation of the elements. At the same time, numerous depressions and furrows evidence the plastic character of the cracks.
6. Fractographic analysis in two load conditions and four combinations of bending and torsion shows that as a result of higher loads, i.e., lower durability, the fatigue zone is more pronounced and can be easily distinguished from the static fracture zone.
7. Because the elements of passenger coaches are subjected to variable loads during operation, a material with greater plasticity may be used for windows and doors despite their lower static strength. This is because, in the case of a very large number of cycles to failure, the fatigue strength is comparable.

References

1. Achtelik H., Kurek M., Kurek A., Kluger K., Pawliczek R., Łagoda T. Non-standard fatigue stands for material testing under bending and torsion loading. AIP Conference Proceedings. Mechatronic Systems and Materials 2018; 2029(1): 020001-1-020001-14, https://doi.org/10.1063/1.5066463.
2. Asseala S.A., Gomaa F.R. Fatigue life estimation of 6061 aluminium alloy based on modal damping measurements. Engineering Research Journal 2005; 38: 395-406, https://doi.org/10.21608/ERJM.2005.70255.
3. ASTM E 739–91. Standard practice for statistical analysis of linearized stress–life (S–N) and strain life fatigue data (in): Annual Book of ASTM Standards. Philadelphia, Press: 1999; 614–628.

4. Beretta S., Murakami Y. Statistical analysis of defects for fatigue strength prediction and quality control of materials. Fatigue & Fracture of Engineering Materials & Structures 1998; 21: 1049–1065, https://doi.org/10.1046/j.1460-2695.1998.00104.x.
5. Blacha Ł., Karolczuk A., Bański R., Stasiuk P. Application of the weakest link analysis to the area of fatigue design of steel welded joints. Engineering Failure Analysis 2013; 35: 665-677, https://doi.org/10.1016/j.engfailanal.2013.06.012.
6. Blacha Ł., Karolczuk A. Validation of the weakest link approach and the proposed Weibull based probability distribution of failure for fatigue design of steel welded joints. Engineering Failure Analysis 2016; 67: 46-62, https://doi.org/10.1016/j.engfailanal.2016.05.022.
7. Boni L., Lanciotti A., Polese C. "Size effect" in the fatigue behavior of Friction Stir Welded plates. International Journal of Fatigue 2015; 80: 238-245, https://doi.org/10.1016/j.ijfatigue.2015.06.010.
8. Borrego L.P., Abreu L.M., Costa J.M., Ferreira J.M. Analysis of low cycle fatigue in AlMgSi aluminium alloys. Engineering Failure Analysis 2004; 11: 715–725, https://doi.org/10.1016/j.engfailanal.2003.09.003.
9. Carpinteri A., Spagnoli A., Sabrina Vantadori S. Size effect in S–N curves: A fractal approach to finite-life fatigue strength. International Journal of Fatigue 2009; 31(5): 927-933, https://doi.org/10.1016/j.ijfatigue.2008.10.001.
10. Da Silva L.F., Ochsner A., Adams R.D. (Editors). Handbook of Adhesion Technology, Vol. 2, Springer. Press: 2011. https://doi.org/10.1007/978-3-642-01169-6
11. EN 515:2017-05 - Aluminium and aluminium alloys – Wrought products – Temper designations.
12. EN 573-1 - 2004- Aluminium and aluminium alloys - Chemical composition and form of wrought products - Part 1: Numerical designation system.
13. EN 755-2 - 2016 - Aluminium and aluminium alloys - Extruded rod/bar, tube and profiles - Part 2: Mechanical properties.
14. Fang Y., Zhang Y.(H) (Editors). China's High-Speed Rail Technology, An International Perspective, Advances in High-speed Rail Technology. Springer, Zhejiang University Press. https://doi.org/10.1007/978-981-10-5610-9.
15. Farmer S. M. Aluminum Fatigue: A literature review covering its influence on engineering from design to end of service. Master of Engineering in Aerospace Engineering, Blacksburg, Virginia. Press: 2022.
16. Feng G., Shengchuan W.,Jianxin L., Zhengkai W., Shanqiang F., Sansan D. A time-domain stepwise fatigue assessment to bridge small-scale fracture mechanics with large-scale system dynamics for high-speed maglev lightweight bodies. Engineering Fracture Mechanics 2021; 248:107711, https://doi.org/10.1016/j.engfracmech.2021.107711.
17. Gou G., Zhanga M., Chena H., Chena J., Li P., Yang Y.P. Effect of humidity on porosity, microstructure, and fatigue strength of A7N01S-T5 aluminum alloy welded joints in high-speed trains. Materials and Design 2015;85:309–317, http://dx.doi.org/10.1016/j.matdes.2015.06.177.
18. Gough H.J., Pollard H.V., Clenshaw W.J. Some experiments on the resistance of metals to fatigue under combined stresses. Aero Research Council, London, Rand m 2522, H.M.S.O. Press: 1951.
19. Hockaufa K., Niendorf T., Wagner S., Halle T., Meyer L.W. Cyclic behavior and microstructural stability of ultrafine-grained AA6060 under strain-controlled fatigue. Procedia Engineering 2010; 2: 2199–2208, https://doi.org/10.1016/j.proeng.2010.03.236.
20. Janutienė R., Mažeika D.. Analysis and fracture of aluminium alloy components used for spinning of chemical fiber. International Scientific Journal "Machines. Technologies. Materials" 2018; 6: 251-254.
21. Jha S.K., Balakumar D., Paluchamy R. Experimental Analysis of Mechanical Properties on AA 6060 and 6061 Aluminum Alloys International Journal of Engineering Research and Applications 2015; 5(4): 47-53.
22. Kazymyrovych V. Very high cycle fatigue of engineering materials. Karlstad University Studies 2009:22.
23. Klawonn A., Hagenackera N, Beck T. A probabilistic Haigh diagram based on a weakest link approach. International Journal of Fatigue 2015; 133: 105419, https://doi.org/10.1016/j.ijfatigue.2019.105419.
24. Kowalski A., Ozgowicz W., Grajcar A., Lech-Grega M., Kurek A. Microstructure and Fatigue Properties of AlZn6Mg0.8Zr Alloy Subjected to Low-Temperature Thermomechanical Processing. Metals 2017; 7(10): 448, https://doi.org/10.3390/met7100448.
25. Kowalski A., Ozgowicz W., Jurczak W., Grajcar A., Boczkal S., Kurek A. Microstructural and Fractographic Analysis of Plastically Deformed Al-Zn-Mg Alloy Subjected to Combined High-Cycle Bending-Torsion Fatigue. Metals 2018; 8(7): 487, https://doi.org/10.3390/met8070487.
26. Kucukrendeci I. Mechanical and microstructural properties of EN AW-6060 aluminum alloy joints produced by friction stir welding.

Bulletin of The Polish Academy of Sciences Technical Sciences 2015; 63(2): 475-478, https://doi.org/10.1515/bpasts-2015-0054.

27. Li Z., Wang Q., Luo A.A., Fu P., Peng L. Fatigue strength dependence on the ultimate tensile strength and hardness in magnesium alloys. International Journal of Fatigue 2015; 80: 468–476, https://doi.org/10.1016/j.ijfatigue.2015.07.001.
28. Lindström S.B., Moverare J., Xu J., Leidermark D., Eriksson R., Ansell H., Kapidžić Z. Service-life assessment of aircraft integral structures based on incremental fatigue damage modeling. International Journal of Fatigue 2023;172:107600, https://doi.org/10.1016/j.ijfatigue.2023.107600.
29. Lu Y., Zheng H., Zeng J., Chen T., Wu P. Fatigue life reliability evaluation in a high-speed train bogie frame using accelerated life and numerical test. Reliability Engineering and System Safety 2019;188:221–232, https://doi.org/10.1016/j.ress.2019.03.033.
30. Małecka J., Łagoda T. Fatigue and fractures of RG7 bronze after cyclic torsion and bending,. International Journal of Fatigue 2023; 168: 107475, https://doi.org/10.1016/j.ijfatigue.2022.107475.
31. Miao B.R., Luo Y.X., Peng Q.M., Qiu Y.Z., Chen H., Yang Z.K. Multidisciplinary design optimization of lightweight carbody for fatigue assessment. Materials and Design 2020;194:108910, https://doi.org/10.1016/j.matdes.2020.108910.
32. Morgadoa T., Paulo D., Velhinhoe A., Pereiraf M., Mourao A. Fatigue Limit Prediction Models of 6060 Aluminium Extruded Alloy. Procedia Structural Integrity 2022; 42: 1545–1551, https://doi.org/10.1016/j.mspro.2014.06.150.
33. NI Y-Q., YE XW (Editors). Proceedings of the 1st International Workshop on High-Speed and Intercity Railways. Lecture Notes in Electrical Engineering. Volume 147, Springer. Press: 2012. https://doi.org/10.1007/978-3-642-27963-8
34. Nickel D., Dietrich D., Mehner T., Frint P., Spieler D., Lampke T. Effect of Strain Localization on Pitting Corrosion of an AlMgSi0.5 Alloy. Metals 2015; 5(1): 172-191, https://doi.org/10.3390/met5010172.
35. Sung S., Park C.S., Kim K.H., Shin B.C., Min A.K. Fatigue Strength Evaluation of the Aluminium Carbody of Urban Transit Unit by Large Scale Dynamit Load Test. JSME International Journal 2005, Series A; 48 (1). https://doi.org/10.1299/jsmea.48.27
36. Telesman J. Review of the Effects of Micro structure on Fatigue in Aluminum Alloys. NASA Technical Memorandum 83626, Lewis Research Center, Cleveland, Ohio. Press: 1984.
37. Transport Systems And Technologies. Collection of Scientific Papers of the State University of Infrastructure and Technologies Series: Transport Systems and Technologies. Ministry of Education and Science of Ukraine State University of Infrastructure and Technologies, Issue 41, Kyiv. Press: 2023.
38. Wagener R., Melz T. Fatigue life curve – A continuous Wöhler curve from LCF to VHCF. Fatigue Testing 2018; 10: 924-930, https://doi.org/10.3139/120.111233.
39. Weigang H., Zhiming L., Dekun L., Xue H. Fatigue failure analysis of high speed train gearbox housings. Engineering Failure Analysis 2017;73: 57–71, http://dx.doi.org/10.1016/j.engfailanal.2016.12.008.
40. Weiyuan D., Lele Z., Haifeng C., Haifeng Z., Changqing L. Fatigue Characterization on a Cast Aluminum Beam of a High-Speed Train Through Numerical Simulation and Experiments. Chinese Journal of Mechanical Engineering 2021; 34:108, https://doi.org/10.1186/s10033-021-00628-6.
41. Winter L., Hockauf K., Lampke T. Mean stress sensitivity of the fatigue strength after equalchannel angular pressing of the aluminum alloys 6082 and 6060. IOP Conf. Series: Materials Science and Engineering 2019; 480: 012032, https://doi.org/10.1088/1757-899X/480/1/012032.
42. Yaohui L., Penglin X., Dongb P., Xing Z., Jing Z. Analysis of the effects of vibration modes on fatigue damage in high-speed train bogie frames. Engineering Failure Analysis 2018;89: 222–241, https://doi.org/10.1016/j.engfailanal.2018.02.025.
43. Zhengkai W., Xiru Z. Tensile and fatigue behaviors of hybrid laser welded A7N01 alloy with repairing for railway vehicles. Engineering Failure Analysis 2023;143:106930, https://doi.org/10.1016/j.engfailanal.2022.106930.

This study was financially supported by the Opole University of Technology under DELTA project no. 140/22